ALG-2 interacting protein-X (Alix) is required for activity-dependent bulk endocytosis at brain synapses

Marine H. Laporte [1,2,*], Kwang Il Chi[1*], Laura C. Caudal[3], Na Zhao[3], Marta Rolland[1], , José Martinez-Hernandez[1,4], Magalie Martineau[5], Christine Chatellard[1,6] Eric Denarier[1], Vincent Mercier[1,7], Florent Lemaître [1,8], Béatrice Blot[1], Eve Moutaux[1], Maxime Cazorla[1,9], David Perrais[5], Fabien Lanté[1], Sandrine Fraboulet[1,10] , Fiona J. Hemming[1], Frank Kirchhoff[3], Rémy Sadoul[1,6£]

1) Grenoble Institute Neurosciences, University Grenoble Alpes- INSERM U1216- CEA, Grenoble, France
2) Department of Cell Biology, University of Geneva, Geneva, Switzerland.
3) Molecular Physiology, Center for Integrative Physiology and Molecular Medicine (CIPMM), University of Saarland, Homburg, Germany.
4) Department of Biochemistry and Molecular Biology, Faculty of Science and Technology, University of the Basque Country (UPV/EHU), Leioa, Spain.
5) Interdisciplinary Institute for Neuroscience, University of Bordeaux-CNRS UMR 5297, Bordeaux, France
6) Institut de Biologie Structurale, University Grenoble Alpes- CNRS-CEA UMR 5075, Grenoble, France
7) Department of Biochemistry, University of Geneva, Geneva, Switzerland.
8) Département des Neurosciences, Centre de Recherche du centre hospitalier de Montréal, Canada
9) Institut de Neuroscience la Timone, CNRS UMR7289, Marseille, France
10) Institute for Advanced Biosciences, Univ. Grenoble Alpes - INSERM U1209 - CNRS UMR 5309, Grenoble, France

*Equal contribution
£Corresponding author
email: remy.sadoul@univ-grenoble-alpes.fr

Running title: Alix and ADBE

Number of pages: 35
Items number: 7 figures, 2 movies.
Words count: abstract (176), introduction (660), discussion (1164).

Abstract

In chemical synapses undergoing high frequency stimulation, vesicle components can be retrieved from the plasma membrane via a clathrin-independent process called activity dependent bulk endocytosis (ADBE). Alix (ALG-2 interacting protein X)/ PDCD6IP) is an adaptor protein binding to ESCRT and endophilin-A proteins which is required for clathrin-independent endocytosis in fibroblasts. Alix is expressed in neurons and concentrates at synapses during epileptic seizures. Here, we used cultured neurons to show that Alix is recruited to presynapses where it interacts with, and concentrates endophilin-A during conditions triggering ADBE. Using Alix knockout (ko) neurons we showed that this recruitment, which requires interaction with the calcium-binding protein ALG-2, is necessary for ABDE. We also found that presynaptic compartments of Alix ko hippocampi display subtle morphological defects compatible with flawed synaptic activity and plasticity detected electrophysiologically. Furthermore, mice lacking Alix in the forebrain undergo less seizures during kainate-induced status epilepticus and reduced propagation of the epileptiform activity. These results thus show that impairment of ADBE due to the lack of neuronal Alix alters synaptic recovery during physiological or pathological repeated stimulations.

Keywords: PDCD6IP**,** Clathrin-independent-endocytosis, Alix knock-out, endophilin-A, ALG-2, bulk endocytosis, synaptic vesicle recycling, synaptic transmission, calcium, epileptic seizures.

Introduction

Neuronal communication in mammalian brain relies heavily on the activity-dependent release of chemical neurotransmitters from presynaptic boutons. Following fusion of synaptic vesicles (SV) with the presynaptic membrane, SV lipids and proteins are retrieved by endocytosis. Endocytosis avoids detrimental increase in the plasma membrane surface and allows recycling of the SV components to replenish the SV pool (Gan and Watanabe, 2018). At moderate levels of stimulation, retrieval of membrane involves clathrin-mediated (CME) and clathrin-independent endocytosis (CIE), in proportions which are still highly debated (Chanaday and Kavalali, 2018). Moreover, long-lasting high-frequency stimulations also lead to the clathrin-independent internalization of large stretches of presynaptic membranes. This calcium-dependent process, first discovered at the amphibian neuromuscular junction (Miller and Heuser, 1984) is referred to as activity-dependent bulk endocytosis (ADBE). It is meant to avoid abnormal increase of the synaptic bouton surface and to allow replenishment of SVs during sustained synaptic stimulations (Cheung and Cousin, 2012; Marxen et al., 1999). Thus, ADBE has been suggested to play key regulatory roles in physiological or pathological events like epilepsy, which are triggered and sustained by high frequency neuronal activity. However, decrypting the physiological role of ADBE has been hindered by the lack of identified molecules that are both specific and essential to this endocytosis mode.

We have recently demonstrated that ALG-2 interacting protein-X (Alix) is essential for clathrin-independent bulk endocytosis in fibroblasts (Mercier et al., 2016). Alix ko mice have normally organized but smaller brains (Campos et al., 2016; Laporte et al., 2017), a phenotype linked with an alteration of CIE in developing neurons (Laporte et al., 2017). In the adult brain, Alix is ubiquitously expressed but concentrates at hippocampal presynaptic terminals during epileptic seizures (Hemming et al., 2004). Alix is a cytosolic protein first identified through its calcium-dependent binding to the penta-EF-hand protein ALG-2 (apoptosis-linked gene 2) which helps opening and activating the protein (Chatellard-Causse et al., 2002; Missotten et al., 1999; Sadoul, 2006). Its activation leads to interaction with membranes as reported in the case of plasma membrane wounds, where ALG-2 binds to inflowing calcium and helps recruiting Alix to the membrane where the latter organizes repair (Scheffer et al., 2014). Alix also interacts with lipids (Bissig et al., 2013) and with several membrane modifying proteins among which endophilin-A proteins (A1, A2 and A3) (Chatellard-Causse et al., 2002). These

91 cytoplasmic proteins that contain an N-BAR (Bin/Amphiphysin/Rvs) domain capable of sensing
92 and generating membrane curvature (Kjaerulff et al., 2011), are major actors of CME at
93 synapses (Gad et al., 2000; Ringstad et al., 1999). They also drive CIE in fibroblasts (Boucrot et
94 al., 2014; Renard et al., 2014) and were shown to control the fast mode of CIE at ribbon
95 synapses (Llobet et al., 2011) as well as in hippocampal neurons (Kononenko et al., 2014;
96 Watanabe et al., 2018).

97 The role of Alix in bulk endocytosis in fibroblasts, its capacity to interact with endophilin-A
98 and to be recruited by calcium at membranes, together with its increased concentration at
99 hippocampal synapses during kainate-induced seizures, brought us to test its possible function
100 in ADBE.

101 Using cultured wildtype (wt) neurons, we now bring evidence that sustained synaptic
102 activity leads to calcium-dependent recruitment of ALG-2 at synapses. ALG-2 in turn interacts
103 with Alix, which binds and concentrates endophilin-A. This protein complex is necessary for
104 ADBE, which is selectively impaired in Alix ko neurons. We also report that synapse
105 morphology and function are both altered in Alix ko brains. This finding correlates with the
106 modifications in kinetics of synaptic recovery following prolonged stimulation that we
107 detected in hippocampal slices of mice in which Alix was selectively deleted in forebrain
108 neurons. In these mice, the number of seizures during status epilepticus induced by
109 intracortical kainate injections was reduced as well as the propagation of epileptiform activity
110 to the contralateral side of injection. Thus, our results show that some molecular mechanisms
111 involved in ADBE may also be involved in certain aspects of synaptic plasticity such as short-
112 term synaptic depression and recurrence of epileptic seizures.

113 **Material and methods**

114

115 Plasmids

116 Endophilin A2-mCherry was obtained by subcloning (In-Fusion Cloning kit, Clontech)
117 endophilin A2 cDNA into a pmCherry-N1 vector (Clontech). GFP-ALG-2 was obtained by
118 performing a reverse mutagenesis (Quick change II site directed mutagenesis kit, Stratagene)
119 on a GFP-hALG-2 Y180A (a generous gift from Masatoshi Maki) to acquire GFP-hALG-2wt.
120 hALG-2 E47A-E114A cDNA was kindly provided by Masatoshi Maki (Shibata et al., 2004) and
121 was subcloned into a pEGFP-C1 vector (Clontech) to obtain GFP-hALG-2 E47A-E114A (GFP-
122 ALG-2ΔCa).

123 All constructs containing Alix cDNA (wt or mutants) were obtained by subcloning the relevant
124 cDNAs from pCI vectors harbouring Alix cDNA or its mutants. Alix I212D (AlixΔCHMP4B) and
125 AlixΔPGY (AlixΔALG-2) cDNAs in pCI were generated by mutagenesis (Quick change II site
126 directed mutagenesis kit, Stratagene) and Alix R757E (AlixΔendo) by in-fusion cloning, using
127 the oligos given below.

128 mCherry-2Xflag-mAlix wt (mCherry-Alix) was obtained by subcloning 2xflag-mAlix wt cDNA
129 into a pmCherry-C1 vector (Clontech). Alix-YFP was obtained by subcloning wild type Alix
130 cDNA into a pEYFP-N1 vector (Clontech). GFP-flag-Alix (GFP-Alix) was described in (Mercier et
131 al., 2016). GFP-Alix and its mutant forms (GFP-Alix R757E, GFP-AlixΔPGY) were obtained by
132 subcloning the various cDNAs into a pEGFP-C1 vector (Clontech). DNA constructs used for the
133 rescue experiments were prepared in two steps. First, IRES2-GFP cDNA was subcloned into
134 pSIN lentiviral vector (kindly provided by F. Saudou) by using pIRES2-GFP (Clontech) as a
135 template. Then the various cDNAs were subcloned into pSIN-IRES2-GFP.

136 Oligos used to generate mutants:

137 Alix I212D

138 sense: 5'-AAGATGAAAG ATGCCGACAT AGCTAAGCTG-3'

139 antisense: 5'-CAGCTTAGCT ATGTCGGCAT CTTTCATCTT -3'

140 Alix R757E

141 sense: 5'-CAGCCGAGCC TCCACCTCCT GTGCTTCCTG -3'

142 antisense: 5'-GAGGCTCGGC TGGAGGCTGG GGCTTAGCAG-3'

143 AlixΔPGY

144 sense: 5'-GCCACAGGCT CAGGGATGCC AAATGCCCAT GC-3'

145 antisense: 5'-GCATGGGCAT TTGGCATCCC TGAGCCTGTG GC -3'.

146 Antibodies

147

Antibody	Supplier (reference)	Species (type)	Dilution
Anti-Actin	Millipore (MAB1501R)	Mouse (monoclonal)	1/10000
Anti-Alix	Covalab (ab0204)	Rabbit (polyclonal)	1/10000
Anti GFAP	Abcam	Goat (polyclonal)	1/1000
Anti Iba1	Wako	Rabbit (polyclonal)	1/500
Anti-phospho-p44/42 MAPK (T202/Y204)	Cell signaling (9106)	Mouse (monoclonal)	1/1000
Anti-PSD95	NeuroMab (73-028)	Mouse (monoclonal)	1/2000
Anti-PSD95	Millipore (MAB1598)	Mouse (monoclonal)	1/500
Anti-Synapsin-1	Millipore (AB1543P)	Rabbit (polyclonal)	1/1000
Anti-Synaptophysin	Merck Millipore (MAB5258)	Mouse (monoclonal)	1/5000
Anti-Flag	Sigma-Aldrich (F3165)	Mouse (monoclonal)	1/1000
Anti-Flag	Sigma-Aldrich (F7425)	Rabbit (polyclonal)	1/1000
Anti-Mouse HRP	Jackson ImmunoResearch (115-035-166)	Goat (polyclonal)	1/5000
Anti-Rabbit HRP	Jackson ImmunoResearch (115-035-044)	Goat (polyclonal)	1/5000
Anti-Mouse Alexa Fluor 488	Invitrogen (A-11029)	Goat (polyclonal)	1/1000
Anti-Mouse Alexa Fluor 594	Invitrogen (A-11032)	Goat (polyclonal)	1/1000
Anti-Mouse Cy5	Jackson ImmunoResearch (115-175-146)	Goat (polyclonal)	1/500
Anti-Rabbit Alexa Fluor 488	Invitrogen (A-11034)	Goat (polyclonal)	1/1000
Anti-Rabbit Alexa Fluor 594	Invitrogen (A-11037)	Goat (polyclonal)	1/1000
Anti-Rabbit Cy5	Jackson ImmunoResearch (111-175-144)	Goat (polyclonal)	1/1000

148

149 Animals

150 Animals were handled and killed in conformity with European law and internal

151 regulations of INSERM. Pregnant Oncins France souche A (OFA; a substrain of Sprague Dawley)
152 rats (Charles River) were used for rat neuronal cultures. Alix ko C57BL/6 mouse pups (Laporte
153 et al., 2017; Mercier et al., 2016) and their control littermates referred to thereafter as Alix
154 wt, were also used for primary neuronal culture. Transgenic mice were held at the animal
155 facility of the Grenoble Institute for Neurosciences and fed *ad libitum*. All animals were held
156 at a twelve-hour light/dark cycle. One- to two-month-old Alix wt and Alix ko mice were used
157 for electrophysiological extracellular recordings, histochemistry and electron microscopy
158 studies.
159 Mice were anesthetized by intraperitoneal injection of 0.1 ml sodium pentobarbital (5.6% w/v;
160 CEVA Santé Animale) and treated as described in the corresponding sub-headings of the
161 material and methods section.
162 Emx1^{IREScre}/Alix$^{fl/fl}$ and Emx1^{IREScre} control mice, thereafter referred to control and Alix
163 cko, were used for the kainate injection epilepsy model and the electrophysiological. 8-11
164 weeks old mice were anesthetized under a mixture of 2 % isoflurane, 47.5 % O_2 and 47.5 %
165 N_2O. Transgenic mice were held at the animal facility of the CIPMM and fed *ad libitum*. All
166 animals were held at a twelve-hour light/dark cycle. This study was carried out in strict
167 accordance with the European and German guidelines for the welfare of experimental
168 animals. Animal experiments were approved by the Saarland state's "Landesamt für
169 Gesundheit und Verbraucherschutz" animal licence number 36/2016.
170
171 Golgi staining
172 2-month-old anesthetized mice were dislocated prior to brain dissection and 100 µm
173 thick coronal brain sections were cut on a vibratome in the hippocampal region. The dendritic
174 spines of hippocampal neurons from the CA1 *stratum radiatum* were visualized by the Golgi
175 impregnation technique. For this, we used the FD Rapid GolgiStain kit (FD NeuroTechnologies).
176 Brain sections were immersed in equal volumes of solutions A and B for 7 d and impregnated
177 with solution C for 48 h at 4°C. Then, the sections were washed twice in double-distilled water
178 and incubated for 10 min in a mixture solution D and solution E in double-distilled
179 water(1:1:2). Sections were washed twice, dehydrated with increasing concentrations of
180 ethanol, and mounted with epoxy resin (Fluka). Stacks of bright-field images with 0.3 µm
181 spacing were acquired with a Zeiss Axioskop 50 microscope with 63x oil objective (NA 1.4;
182 Plan-Apochromat) coupled to a CCD camera (CoolSnap ES; Roper Scientific) operated by

183 Metaview software (Molecular Devices). Images were analysed with ImageJ. The number of
184 dendritic spines (>1 μm protrusion) along portion of dentrite of 100 μm was counted with
185 ImageJ.
186
187 Transmission electron microscopy of the CA1 hippocampus
188 2-month-old mice mice were anesthetized and intracardially perfused with phosphate-
189 buffered 0.9% NaCl (PBS), followed by 0.1 M phosphate buffered 4% paraformaldehyde, pH
190 7.4, supplemented with 0.05% glutaraldehyde (Sigma). The brains were carefully removed,
191 postfixed for 4 h in the same fixative and 60 μm sections were cut with a vibratome. After
192 several washes in PBS, the sections were postfixed in 1% glutaraldehyde in the same buffer
193 for 10 min and processed for EM. This included treatment with osmium tetroxide (1% in 0.1
194 M PB), block staining with uranyl acetate, dehydration through a graded series of ethanol, and
195 flat embedding on glass slides in Durcupan (Fluka) resin. Regions of interest were cut at 70 nm
196 on an ultramicrotome (Reichert Ultracut E; Leica) and collected on one-slot copper grids.
197 Staining was performed on drops of 1% aqueous uranyl acetate, followed by Reynolds's lead
198 citrate. EM images were acquired in a JEOL-1200 electron microscope with a digital camera
199 (Veleta, SIS; Olympus) and analysed with ImageJ. Twenty images per animal from 3 animals
200 per genotype were used for quantification. The number of synapses per μm^2 was calculated.
201 A synapse was considered if it met 3 criteria: a presynaptic bouton filled with at least 10
202 synaptic vesicles (1) juxtaposed to the head of a dendritic spine with a clearly visible PSD (2)
203 and the presence of the neck in the section (3). Number of synaptic vesicles and areas of
204 presynaptic boutons were quantified in each synapse using the free-shape tool and the cell
205 counter plugins of ImageJ. We used the straight tool of ImageJ to measure the lengths of PSDs,
206 and head and neck diameters. Note that the head diameter was taken parallel to the PSD and
207 the neck diameter was perpendicular to the neck membranes.
208
209 Electrophysiological recordings in CA1
210 *Field recordings*
211 Alix wt and ko brain slices were prepared from 2-month-old C57BL/6 wt and Alix ko mice. The
212 brains were removed quickly and 350 μm-thick sagittal slices containing both cortex and
213 hippocampus were cut in ice-cold sucrose solution (2.5 mM KCl, 1.25 mM NaH_2PO_4, 10 mM
214 $MgSO_4$, 0.5 mM $CaCl_2$, 26 mM NaHCO3, 234 mM sucrose, 11 mM glucose, saturated with 95%

215 O_2 and 5% CO_2) with a Leica VT1200 blade microtome (Leica Microsystemes, Nanterre,
216 France). After cutting, hippocampi were extracted from the slice and transferred to
217 oxygenated Artificial Cerebro-Spinal Fluid (ACSF: 119 mM NaCl, 2.5 mM KCl, 1.25 mM
218 NaH_2PO_4, 1.3 mM $MgSO_4$, 2.5 mM $CaCl_2$, 26 mM $NaHCO_3$, 11 mM glucose) at 37± 1°C for 30
219 min and then kept at room temperature for at least 1 h before recordings. Each slice was
220 individually transferred to a submersion-type recording chamber and continuously superfused
221 (2 ml/min) with oxygenated ACSF. Extracellular recordings were obtained at 28°C from the
222 apical dendritic layers of the hippocampal CA1 area, using glass micropipettes filled with ACSF.
223 Field excitatory postsynaptic potentials (fEPSPs) were evoked by the electrical stimulation of
224 Schaffer collaterals afferent to CA1. The magnitude of the fEPSPs was determined by
225 measuring their slope. Signals were acquired using a double EPC 10 Amplifier (HEKA Elektronik
226 Dr. Schulze GmbH, Germany) and analysed with Patchmaster software (HEKA Elektronik Dr.
227 Schulze GmbH, Germany). For the induction of long-term potentiation, test stimuli were
228 delivered once every 15 s. Stimulus intensities were adjusted to produce 40-50% of the
229 maximal response. A stable baseline was recorded for at least 15 min. LTP was induced by high
230 frequency stimulation (4 trains delivered at 100 Hz with 5 min between each train). Average
231 value of fEPSP slope was expressed as a percentage of the baseline response.

232 *Patch-clamp recordings*

233 $Alix^{fl/fl}$ mice (Laporte et al., 2017) with heterozygous cre expression ($Emx1^{IREScre}$
234 ($Emx^{tm1(cre)Krj}$, MGI: 2684610)(Gorski et al., 2002) as well as control mice ($Alix^{fl/fl}$ x Emx^{wt}) were
235 decapitated under anaesthesia and brains were removed from the skull and immersed in an
236 ice-cold, oxygenated (5% CO_2/95% O_2, pH 7.4) slice preparation solution containing (in mM)
237 87 NaCl, 3 KCl, 25 $NaHCO_3$, 1.25 NaH_2PO_4, 3 $MgCl_2$, 0.5 $CaCl_2$, 75 sucrose and 25 glucose.
238 Coronal slices of 300 µm thickness were prepared with a vibratome (Leica VT 1200S, Nussloch,
239 Germany) and transferred to a nylon basket slice holder for incubation in ACSF containing (in
240 mM) 126 NaCl, 3 KCl, 25 $NaHCO_3$, 15 glucose, 1.2 NaH_2PO_4, 2 $CaCl_2$, and 2 $MgCl_2$ at 32 °C for
241 30min. Subsequently, slices were removed from the water bath and kept at room temperature
242 with continuous oxygenation prior to use.

243 Slices were transferred to the recording chamber continuously perfused with
244 oxygenated ACSF containing (in mM) 1 $MgCl_2$ and 2.5 $CaCl_2$ (2-5 mL/min). During recordings,
245 50 µM strychnine and 50 µM picrotoxin were added to block inhibitory synaptic transmission.
246 Pyramidal neurons were identified morphologically using the recording microscope (Axioskop

247 2 FS mot, Zeiss, Jena, Germany) with a 40x water immersion objective. Images were detected
248 with a QuantEM 512SC camera (Photometrics, Tucson, USA). Whole-cell membrane currents
249 were recorded by an EPC 10 USB amplifier (HEKA, Lambrecht, Germany), low pass filtered at
250 3 kHz and data acquisition was controlled by Patchmaster software (HEKA). The resistance of
251 patch pipettes (7–9 ΩM) were fabricated from borosilicate capillaries (OD: 1.5 mm; Sutter,
252 USA) using a Micropipette Puller (Model P-97, Sutter Instrument Co., CA). Patch pipettes were
253 filled with a solution containing (in mM) 125 cesium gluconate, 20 tetraethylammonium (TEA),
254 2 $MgCl_2$, 0.5 $CaCl_2$, 1 EGTA, 10 HEPES and 5 Na_2ATP (pH 7.2). The holding potential in voltage-
255 clamp mode was at -70 mV. Spontaneous excitatory postsynaptic currents (sEPSC) were
256 recorded under holding potential for 40 seconds in 5 minutes later after whole-cell
257 configuration. Here only <=-10 pA sEPSC was analyzed. Excitatory postsynaptic currents
258 (EPSCs) of pyramidal neurons in the hippocampal CA1 were evoked by stimulating Schaffer
259 collaterals of CA3 neurons with a concentric bipolar microelectrode (MicroProbes, USA).
260 Stimulus duration was 200 µs. To estimate short-term plasticity, 25 trains of stimuli were
261 applied to induce synaptic depression, and the depressing trains were repeated at 10 Hz with
262 an interval of 20 s to allow for recovery from synaptic depression. To investigate recovery from
263 depression, stimulation with gradually increased interval was applied. The stimulation
264 threshold was applied from 30 µA to 80 µA. All the experiments were conducted at room
265 temperature (RT) (22 – 24 ℃).
266 Data generated by Patch Master were loaded into Matlab (Mathworks, MA, USA) with
267 a module adapted from sigTOOL (Lidierth, 2009). EPSC traces from the same cells were
268 manually checked and pooled. The average of EPSC traces from each cell was used to analysis.
269 The readily releasable pool (RRP) size was estimated by using train-extrapolation method
270 (Neher, 2015; Thanawala and Regehr, 2016).The cumulative sum of the peak EPSC amplitudes
271 was plotted against the stimulation numbers. The last 10 data points were linearly fitted. The
272 RRP size was calculated by back-extrapolating the fitted line to the y-axis (stimulation ID = 0).
273 The release probability was calculated by p = Amplitude^1 / RRP_{train}. The fitted slop represents
274 the replenishment rate (Körber et al., 2015). The recovery was estimated with the decay
275 constant (τ) as $N_t = N_0 * exp\left(-\frac{t}{\tau}\right)$.
276 Data analysis was performed using routines that were custom written in Matlab.
277

278 EEG telemetry and unilateral intracortical kainate injection

279 We took advantage of the unilateral intracortical kainate injection model for human temporal
280 lobe epilepsy. Telemetric EEG transmitter implantation, kainate injection and data analysis
281 was adapted from Bedner and colleagues (Bedner et al., 2015).

282 Controls and alix cko were implanted with telemetric EEG transmitters (DSI PhysioTel®
283 ETA-F10, Harvard Bioscences, Inc. Holliston, Massachusetts, USA). The animals were placed in
284 a stereotaxic frame (Robot stereotaxic, Neurostar, Tübingen, Germany) for implantation of
285 depth electrodes at 3.4 mm posterior to bregma and bilaterally 1.6 mm from the sagittal
286 suture. After post-surgical care and recovery, mice were again placed in the stereotaxic frame
287 and injected with 70 nl of a 20 mM solution of kainate (Tocris, Wiesbaden-Nordenstadt,
288 Germany) in 0.9% NaCl, above the right dorsal hippocampus (1.9 mm posterior to bregma,
289 1.5 mm from sagittal suture and 1.3 mm from skull surface). Kainate was injected at a rate of
290 70 nl/ min with a 10 µl Nanofil syringe (34 GA blunt needle, World Precision Instruments,
291 Sarasota, FL, USA). The syringe was kept in place for 2 min after the injection was completed
292 to avoid liquid reflux.

293 Cages were placed on individual radio receiving plates (DSI PhysioTel® RPC-1, Data
294 Sciences International, St. Paul, USA), which record EEG signals and sent them, together with
295 the video recording (MediaRecorder Software, Noldus Information Technology, Wageningen,
296 Netherlands), to an input exchange matrix (DSI PhysioTel® Matrix 2.0 (MX2), Ponemah
297 software, DSI, Data Sciences International, St. Paul, USA). The animals were monitored for at
298 least 20 h post kainate injection. In our model the mortality rate associated to *status*
299 *epilepticus* is less than 5% in more than 50 mice with different genetic backgrounds over the
300 last 12 months.

301 EEG traces were analysed with the Neuroscore software (Version 3.3.1., Data Sciences
302 International, St. Paul, USA). Electrographic seizures were detected with the spike detection
303 protocol. Subsequently, an additional manual screen was employed to remove artifacts that
304 were eventually picked up. Seizures were characterized by high frequency spiking and ceased
305 with a postictal depression (flattening of EEG). Seizure detection was complemented by
306 synchronized video monitoring. Electrographic seizures were associated with behavioural
307 analogues of Racine stages II-V (Racine, 1972). The total duration of *status epilepticus* was
308 defined from the first electrographic seizure to the first seizure free period lasting 1 h.

309

310 For immunohistochemitry analysis, 40 µm free-floating vibratome sections were
311 incubated for one hour in blocking buffer (5 % HS, 0.3 % Triton X in 1x PBS) at room
312 temperature. Sections were incubated with primary antibodies (see antibodies section)
313 diluted in blocking solution, overnight at 4°C. Secondary antibodies and DAPI (0.025 µg/ml,
314 Sigma) were diluted in blocking buffer and incubated for 2 h at room temperature.
315
316 Cell culture and transfection
317 Cortical and hippocampal neurons from rat E18 embryos and P0 Alix wt and ko mice
318 were prepared as previously described (Faure et al., 2006). Briefly, cortices and hippocampi
319 were dissected from E18 rat embryos or P0 mouse pups, treated with trypsin, and
320 mechanically dissociated. Dissociated cells were seeded at a density of $5 \times 10^4/cm^2$ in 100 mm
321 dishes for cortical neurons and $1.5 \times 10^4/cm^2$ onto acid-washed coverslips (either 14 mm
322 diameter or 25 mm; Marienfeld) in either 4-well plates or P35 dishes (ThermoScientific)
323 precoated for 4 h with 50 µg/ml poly-D-lysine (Sigma). Neurons were plated in DMEM
324 containing 10 unit/mL penicillin, 10 µg/mL streptomycin,0.5 mM L-glutamine and 10% of
325 inactivated horse serum (Invitrogen) Neurons were maintained in water-saturated 95% air/5%
326 CO_2 at 37°C. The seeding medium was replaced after 20 h with serum-free neuronal culture
327 medium (Neurobasal medium containing 2% B27 supplement, 10 unit/mL penicillin, 10 µg/mL
328 streptomycin, and 0.5 mM L-glutamine; Invitrogen). Neurons were transfected at 10 DIV as
329 previously described (Chassefeyre et al., 2015). Briefly, for each P35 dish, 2 µg plasmid DNA,
330 250 mM $CaCl_2$ were mixed with an equal volume of 2x BES-buffered saline and left to
331 precipitate for 20 min at room temperature. Neurons were placed in transfection medium
332 (Minimum Essential Medium containing 0.22% $NaHCO_3$, 20 mM D-glucose and 0.5 mM L-
333 glutamine) supplemented with 2% B27, before the DNA precipitate was added. They were
334 then incubated for 1.5 h at 37°C and 5% CO_2. Neurons were then washed by being placed in
335 transfection medium (pre-warmed to 37°C in 10% CO_2) for 20 min at 37°C and 5% CO_2. Finally,
336 they were transferred back into their conditioned medium.
337 Primary cultures of cerebellar granule neurons (CGN) were prepared from 6-day-old
338 C57BL/6 Alix wt and Alix ko pups as described previously (Trioulier et al., 2004), with some
339 modifications. The cerebella were removed, cleared of their meninges, and cut into 1-mm
340 pieces. They were then incubated at 37°C for 10 min in 0.25% trypsin-EDTA and DNAse (1500
341 U/mL). Trypsin was inactivated and cells were dissociated in culture medium (DMEM

342 containing 10% fetal bovine serum, 2 mM L-glutamine, 25 mM KCl, 10 mM HEPES and 10
343 unit/ml penicillin, 10 μg/ml streptomycin). After filtration on 70 μm cell strainers, neurons
344 were plated at 5.10^5 cell/cm^2 onto poly-D-lysine (10 μg/ml, Sigma) precoated coverslips.
345 Cytosine-β-D-arabinoside (10 μM, Sigma) was added after 1 day in vitro (DIV), to prevent the
346 growth of non-neuronal cells, until 8 DIV when neurons were used for activity dependent bulk
347 endocytosis experiment (see below).
348
349 Multi-electrode array
350 Dissociated hippocampal neurons were resuspended in neuronal medium and plated
351 at a 10^6 cells/cm^2 on poly-L-lysine-coated multi-electrode arrays comprising 59 extracellular
352 recording electrodes and one reference electrode (MEA-60 Multichannel Systems, MCS).
353 Electrodes were 30 μm in diameter and separated by a distance of 200 μm. MEA-60 plates
354 were connected to a 60-channel data acquisition system (USB-MEA64) and associated
355 amplifier (MEA1060-Inv-BC) powered by a PS40W power supply system (MCS, Germany). The
356 recording system was then placed in a humidified incubation chamber at 37°C and 5% CO_2.
357 Neurons were left for 5 min to equilibrate before recording. Basal spontaneous activity was
358 recorded for 3 min prior addition of drugs. Bicuculline (100 μM) and 4-aminopyridine (5 mM)
359 were then added and neuronal activity recorded for another 10 min. Signals were recorded
360 with a 1100 gain, sampled at 20 kHz and analyzed with MC Rack software (MCS, Germany).
361 Raw signals were first filtered with a Butterworth band pass filter (2nd order) between 200
362 and 800 Hz to remove electrical noise and low frequency signals. Spike detection analysis was
363 performed on filtered signals using a threshold of 6 standard deviations to mark out action
364 potentials. Burst events were identified as a minimum of 5 consecutive spikes with an
365 interspike interval lower than 100 ms. The minimum interval time between two bursts was
366 fixed at 1000 ms. Representative traces were exported using custom-made Matlab functions
367 (Matlab 2014b).
368
369 Live imaging of synaptophysin-pHluorin upon electrical stimulation
370 Hippocampal neurons from Alix wt and ko mice were transfected with synaptophysin-
371 pHluorin (Syp-pH) at 6 DIV. The recycling of synaptic vesicles was imaged in a buffer solution
372 containing 120 mM NaCl, 5 mM KCl, 2 mM $CaCl_2$, 2 mM $MgCl_2$, 5 mM glucose, 10 mM HEPES
373 adjusted to pH 7.4 and 270 mOsm/l. Experiments were carried out at 34°C. Neurons were

374 stimulated by electric field stimulation (platinum electrodes, 10 mm spacing, 1 ms pulses of
375 50 mA and alternating polarity at 5-40 Hz) applied by a constant current stimulus isolator (SIU-
376 102, Warner Instruments). The presence of 10 µM 6-cyano-7-nitroquinoxaline-2,3-dione
377 (CNQX) and 50 µM D,L-2-amino-5-phosphonovaleric acid (AP5) prevented recurrent activity.
378 Experiments were performed on an inverted microscope (IX83, Olympus) equipped with an
379 Apochromat N oil 100× objective (NA 1.49). Images were acquired with an electron multiplying
380 charge coupled device camera (QuantEM:512SC; Roper Scientific) controlled by MetaVue7.1
381 (Roper Scientific). Samples were illuminated by a 473-nm laser (Cobolt). Emitted fluorescence
382 was detected after passing a 525/50 nm filter (Chroma Technology Corp.). Time-lapse images
383 were acquired at 1 or 2 Hz with integration times from 50 to 100 ms.
384 Image analysis was performed with custom macros in Igor Pro (Wavemetrics) using an
385 automated detection algorithm as described previously (Martineau et al., 2017). The image
386 from the time series showing maximum response during stimulation was subjected to an "à
387 trous" wavelet transformation. All identified masks and calculated time courses were visually
388 inspected for correspondence to individual functional boutons. The intensity values were
389 normalized to the ten frames before stimulation.
390
391 Live Fluorescence Imaging of Alix and endophilin recruitment to synapses
392 For live imaging of protein recruitment, cultured hippocampal neurons were co-
393 transfected with Alix-mCherry or endophilin-A2-mCherry together with Syp-pH expression
394 vectors 2 to 4 days prior to imaging. All live imaging experiments were performed at 37°C and
395 images were acquired using a spinning disk confocal microscope (AxioObserver Z1) with a 63x
396 oil objective (NA 1.46, Zeiss). Transfected neurons were placed in basal medium for 10 min
397 and then mounted in an imaging chamber (POC-R2 Cell cultivation system, Zeiss). After 2 min
398 in basal medium, a 5x bicuculline/4AP solution was added (final concentration, 100 µM and 5
399 mM, respectively) for stimulation which lasted 5 min and the chamber was perfused with
400 basal medium at 3 ml/min for washing for 5min. ROI were drawn on 'presynapses' defined by
401 spots of synaptophysin-pHluorin that increased during stimulation. Fluorescence values were
402 measured in these ROI and then normalised to the initial fluorescence values (fluorescence
403 values prior to stimulation) using ImageJ.
404
405 Immunofluorescence

406 Cultured hippocampal neurons were fixed for 20 min at room temperature in
407 phosphate-buffered 4% paraformaldehyde supplemented with 4% sucrose. After three
408 washes in PBS, cells were permeabilized and blocked in PBS containing 0.3% Triton X-100 and
409 3% BSA for 15 min at room temperature. Coverslips were incubated for 1–2 h at room
410 temperature with primary antibodies (see 'antibodies' section) diluted in the blocking
411 solution. After washing in PBS, cells were incubated for 1 h with secondary antibodies
412 conjugated to Alexa Fluor 488, Alexa Fluor 594, or Cyanine 5 (Cy5), diluted in the blocking
413 solution. Coverslips were rinsed and mounted in Mowiol. Images were acquired on a Leica SPE
414 microscope using a 40x dry objective (NA 0.75, Leica) or a 100x oil immersion objective (NA
415 1.4, Leica) at 488 nm, 532 nm or 635 nm.
416 *Synapse density*: Cultured hippocampal neurons were fixed and stained with
417 antibodies at 14-16 DIV as described above. Presynaptic boutons (synapsin-1-positive) and
418 postsynaptic terminals (PSD95-positive) were selected using the Spot Detector plugin in Icy
419 software (de Chaumont et al., 2012) (wavelet detection with size filtering between 0.4 µm and
420 2 µm in diameter) on max image projections. Synapses were defined as spots of colocalization
421 between the detected presynaptic and postsynaptic terminals that were within 3 µm of each
422 other. Synapses were counted using the Colocalization Studio in ICY software (Lagache et al.,
423 2018)
424 *Protein recruitment assays*: Cultured hippocampal neurons were transfected with
425 expression vectors 24~48 h prior to stimulation. The transfected neurons were incubated in
426 basal medium (150 mM NaCl, 5 mM KCl, 1.3 mM $CaCl_2$, 10 mM HEPES and 33 mM D-glucose
427 at pH 7.4) for 10 min prior to stimulation. Coverslips were either treated with basal medium
428 alone or bicuculline/4AP solution (basal medium supplemented with 100 µM bicuculline and
429 5 mM 4-aminopyridine) for 5 min at 37°C and 5% CO_2. Coverslips were fixed and stained with
430 antibodies against synapsin-1 and PSD95 (see 'antibodies' section). Images were acquired on
431 a Leica SPE microscope using a 100x oil immersion objective (NA 1.4, Leica). The acquired
432 images were analysed using ImageJ. Regions of interest (ROI) were drawn on areas of axons
433 which colocalize with anti-synapsin-1 spots, but not with anti-PSD95 spots to ensure
434 presynaptic measurement. Fluorescence intensities were then measured in these ROI and
435 normalised to fluorescence intensities measured on other regions of axons to give the relative
436 fluorescence intensity at presynaptic boutons.
437

438 Calcium increase imaging upon neuronal stimulation

439 Hippocampal neurons cultured on 24-well plates were placed in basal medium and
440 incubated with 1 µM Fluo-4-AM for 1 h at 37°C. After washing, neurons were left in 250 µl
441 basal medium for 5 min. Plates were then transferred to a Pherastar automatic plate reader
442 (BMG Labtech, Germany) set to 37 °C, to record fluorescence intensity at 0.1 Hz during 10min,
443 for each well, and with fluorescence measurement settings as described on
444 http://www.bmglabtech.com/media/35216/1043854.pdf. Neurons were stimulated with 50
445 µl 6x bicuculline/4AP solution (final concentration, 100 µM and 5 mM, respectively) after 5min
446 with automatic injection.

447

448 Dextran uptake upon neuronal stimulation

449 The protocol for dextran uptake was adapted from (Clayton and Cousin, 2009b). 15-17
450 DIV hippocampal neurons were stimulated with bicuculline/4AP solution for 5 min, at 37°C
451 and 5% CO_2, in the presence of 10 kDa tetramethylrhodamine-dextran (50 µM). Coverslips
452 were immediately washed several times in washing solution (basal medium supplemented
453 with 0.2% BSA and warmed to 37°C) to remove excess dextran. For ADBE inhibition, neurons
454 were stimulated in the presence of 2 µM GSK3 inhibitor (CT99021, Tocris) and placed in fresh
455 basal medium containing 2 µM GSK3 inhibitor for 10 min at 37°C and 5% CO_2. Neurons were
456 then fixed as previously described and imaged with a Leica SPE microscope using a 40x dry
457 immersion objective (NA 0.75, Leica). Analysis was performed on ImageJ. The number of
458 fluorescent spots was counted in a defined field of view (130µm x 130 µm) in thresholding
459 analysis with a diameter limit between 300 nm and 2 µm (resolution limit for the microscope
460 and maximum size of a nerve terminal).

461 For rescue experiments, cultured hippocampal neurons were transfected 2 to 4 d prior
462 to the day of experiment with the following constructs :Alix wt, Alix I212D (AlixΔCHMP4B),
463 AlixΔPGY (AlixΔALG-2), Alix R757E (AlixΔendo). Dextran uptake assay was performed as
464 described above. Images were acquired on a Leica SPE microscope using a 40x oil immersion
465 objective (NA 1.25, Leica) at 488 nm and 532 mm excitation. The analysis was performed on
466 ICY software. ROI were generated closely around axons by using 'thresholder'. Then dextran
467 spots within these ROI were counted by using 'spot detector' with size limit between 300 nm
468 and 2 µm. The length of axon per field of view was estimated by manually drawing 'Polyline

469 type ROI' over the axon images. The number of dextran spots per µm of axon was calculated
470 and expressed as ratio to control values.
471
472 EM examination of ADBE in culture neurons
473 Analysis of ADBE from cerebellar granule neurons was performed as described
474 previously with some modifications (Cheung et al., 2010). 8 DIV CGN were incubated in
475 hyperpolarizing medium (170 mM NaCl, 3.5 mM KCl, 0.4 mM KH_2PO_4, 20 mM TES, 5 mM
476 $NaHCO_3$, 5 mM D-glucose, 1.2 mM Na_2SO_4, 1.2 mM $MgCl_2$, 1.3 mM $CaCl_2$, pH7.4) for 10 min
477 prior to stimulation. Neurons were then incubated for 2 min with 10 mg/ml HRP (Sigma P8250)
478 in either the hyperpolarizing medium or a high-potassic solution containing 50 mM KCl (123.5
479 mM NaCl, 50 mM KCl, 0.4 mM KH_2PO_4, 20 mM TES, 5 mM $NaHCO_3$, 5 mM D-glucose, 1.2 mM
480 Na_2SO_4, 1.2 mM $MgCl_2$, 1.3 mM $CaCl_2$, pH7.4) before rapid washing in PBS and fixation in PBS-
481 glutaraldehyde 2% for 30 min. After three washes in Tris buffer 100 mM, endocytosed HRP
482 was revealed by incubation in Tris 100 mM containing 0.1% diaminobenzidine and 0.2% H_2O_2.
483 The cultures were then post-fixed in 1% osmium tetroxide, dehydrated and embedded in
484 Epon. Synapses were photographed with a JEOL-1200 electron microscope. Quantification
485 was performed as follows: HRP-positive structures were quantified per synapse and classified
486 as synaptic vesicles when the diameter was less than 100 nm and as bulk endosome when the
487 diameter was more than 100 nm.
488 For focused ion beam scanning electron microscopy (FIB-SEM), the block was mounted
489 on a pin, coated with gold, and inserted into the chamber of a HELIOS 660 Nanolab DualBeam
490 SEM/FIB microscope (FEI Co., Eindhoven, The Netherlands). Region of interest (ROI) was
491 prepared using focused ion beam (FIB) and ROI set to be approximatively 15 µm wide. During
492 the acquisition process, the image acquisition parameters of the electron beam were 2 kV and
493 0.4 nA and the thickness of the FIB slice between each image acquisition was 10 nm. The
494 segmentation of the synapse and ABDE was done with Amira software (Thermo Fisher
495 Scientist) and the movie obtained using Imaris (Oxford Instruments).
496
497 Synaptosomal preparation from cortical neurons
498 Synaptosome-enriched membranes from 15 DIV cortical neurons were prepared as described
499 previously with some modifications (Frandemiche et al., 2014). Briefly, cultured neurons were
500 stimulated for 15 min with a mixture of bicuculline/4AP (50 µM/2.5 mM). After a wash in

501 HBSS, neurons were homogenized by passing 15-20 times through 0.25G needle in cold buffer
502 containing 0.32 M sucrose, 10 mM HEPES, 15mM NaF, 15mM β-glycerophosphate and
503 protease inhibitors (Roche), pH 7.4. Samples were maintained at 4°C during all steps of the
504 experiment. Homogenates were cleared at 1000g for 10 min to remove nuclei and large
505 debris. The resulting supernatants were spun down at 12,000 g for 20 min to obtain a crude
506 membrane fraction and washed twice in HEPES buffer 4 mM containing 1 mM EDTA, 15 mM
507 NaF, 15 mM β-glycerophosphate and protease inhibitors (Roche), pH 7.4. The resulting pellet
508 was solubilized in 0.5% Triton X-100, 20 mM HEPES, 100 mM NaCl, 15mM NaF, 15 mM β-
509 glycerophosphate, pH 7.2, containing protease inhibitors (Roche) for 20 min at 4°C with mild
510 agitation and analysed by Western blot.
511
512 Western blot
513 Cells lysates were resuspended in Laemmli buffer and resolved by SDS-PAGE in 10%
514 polyacrylamide gels. Proteins were electro-transferred onto PVDF membranes that were then
515 blocked for 30 min in TBS containing 0.1% Tween 20 and 5% dry milk and incubated for 1 h to
516 overnight with primary antibodies diluted in the blocking solution. After washes in TBS–
517 Tween, the membranes were further incubated for 1 h with secondary antibodies coupled to
518 HRP, washed as before and incubated with luminescence-generating HRP substrate. Bound
519 antibodies were revealed by luminography on film.
520
521 Statistical analysis
522 The comparison of two groups was performed using two-sided Student's t-test or its non-
523 parametric correspondent, the Mann-Whitney test, if normality was rejected (Shapiro-Wilks
524 test). The comparisons of more than two groups were made using one or two way ANOVAs
525 followed by post-hoc tests (Holm Sidak's or Tukey's HSD) to identify all the significant group
526 differences. N indicates independent biological replicates. The graphs with error bars indicate
527 1 SEM (+/-) except for figure 5 where we used box plots showing distribution of medians
528 (whiskers = min and max values), figures 7 and supplementary figure 6 where median and
529 interquartile range (IQR) were represented. The significance level is denoted as usual
530 (*$p<0.05$, **$p<0.01$, ***$p<0.001$). All the statistical analyses were performed using Prism7
531 (Graphpad version 7.0a, April 2, 2016).
532

533 **Results**

534 Alix is recruited to synapses upon synaptic activation.

535 We used dissociated cortical neuron cultures to decipher the role of Alix at synapses.
536 Western blot analysis during *in vitro* differentiation revealed that Alix expression strongly
537 increases during synaptogenesis as indicated by the parallel rise in postsynaptic density
538 protein 95 (PSD95) expression (**Figure 1A**). Moreover, synaptosome-enriched membranes
539 prepared from mature cortical neurons contained Alix (**Figure 1B**). This synaptic pool
540 increased when neuron cultures were incubated 15 min with the $GABA_A$ receptor antagonist
541 bicuculline, together with a weak potassium channel blocker 4-aminopyridine (4AP)(**Figure**
542 **1B**), a treatment known to increase the frequency of action potential bursts (**Supplementary**
543 **figure 3C**) and thereby induce sustained intracellular calcium elevation (**Supplementary figure**
544 **1A**) (Hardingham et al., 2001; Hardingham et al., 2002). Therefore, this observation suggests
545 that Alix tends to concentrate at synapses undergoing prolonged stimulations. To further
546 confirm this, we used live imaging to follow mCherry-Alix relocalization to synapses in mature
547 hippocampal neurons. While the fluorescent signal was homogeneously distributed
548 throughout the entire neuronal cytoplasm in resting conditions (**Figure 1C**, t= 0 min), it almost
549 doubled in discrete spots within neuronal processes during synaptic activation (**Figure 1C**,
550 t=2m20s arrowheads). These spots correspond to active presynaptic boutons as they were
551 labelled with Synaptophysin-pHluorin (Syp-pH), which becomes fluorescent upon exocytosis
552 at synapses (Granseth et al., 2006) (arrowheads **Figure 1C**; **Movie 1**). Alix recruitment to these
553 sites is concomitant with the activation of glutamatergic synapses, being detectable a few
554 seconds after addition of bicuculline/4AP to the culture medium and decreasing soon after
555 washing the cells (**Figure 1 C, D**). Alix relocalization was also seen with Alix-YFP which
556 concentrated during bicuculline/4AP treatment at sites confirmed to be at axonal boutons by
557 synapsin-1 immunolabelling (**Figure 1E, F**). Anti-PSD95 immunostaining showed that Alix-YFP
558 positive spots were juxtaposed to, but did not overlap with the postsynaptic density marker
559 (**Figure 1G**). Accordingly, measuring Alix-YFP fluorescence intensities in dendritic spines
560 before and during stimulation showed no accumulation of Alix at the post-synaptic level
561 (**Supplementary figure 1B, C**), further demonstrating that synaptic activation leads to Alix
562 recruitment only at presynaptic parts.

563

564 Recruitment of Alix partners, ALG-2 and endophilin-A, at activated synapses

565 In non-neuronal cells, Alix recruitment to plasma membrane depends on calcium binding
566 to ALG-2, a penta-EF-hand containing protein, which thereafter interacts and activates Alix
567 (Scheffer et al., 2014). In neurons, action potential depolarization induces massive and
568 transient calcium accumulation in the bouton, which triggers fusion of SV with the plasma
569 membrane. Adding the intra-cellular calcium chelators BAPTA-AM or EGTA-AM completely
570 abolished Alix-YFP recruitment (**Supplementary figure 2**). Interestingly, GFP-ALG-2
571 concentrated at presynaptic boutons upon synaptic activation, in contrast to an ALG-2 point-
572 mutant unable to bind calcium (ALG-2ΔCa) (Shibata et al., 2004) (**Figure 2A, B**). The use of
573 neurons prepared from Alix ko mice (Laporte et al., 2017; Mercier et al., 2016) showed that
574 ALG-2 recruitment does not depend on Alix, as it concentrates at stimulated synapses of Alix
575 ko neurons at the same level than in wt neurons (**Figure 2B, C** left histograms). On the
576 contrary, Alix recruitment to active synapses is tightly dependent on its capacity to interact
577 with ALG-2, as a mutated version of the protein unable to interact with ALG-2 (AlixΔALG-2)
578 (Suzuki et al., 2008; Trioulier et al., 2004) does not accumulate at presynaptic boutons upon
579 stimulation (**Figure 2C**, right histogram).
580 Among demonstrated interactors of Alix, endophilins-A are main regulators of endocytosis
581 at synapses and impact the number of SVs (Milosevic et al., 2011; Schuske et al., 2003). We
582 therefore tested if endophilins-A could be recruited to active synapses, similarly to Alix and
583 ALG-2. Endophilin-A2-mCherry was mainly detected at presynaptic boutons and its
584 fluorescence increased during bicuculline/4AP treatment (**Figure 2D, E; Movie 2**). Remarkably,
585 no such increase could be seen in Alix ko neurons, whereas Alix deleted of its endophilin
586 binding domain (AlixΔendo) (Chatellard-Causse et al., 2002), was still able to be recruited to
587 synapses upon activation (**Figure 2F**). This strongly suggests that the increase in endophilin
588 concentration during sustained synaptic activation requires Alix expression.
589 <u>Alix is required for ADBE</u>
590 Altogether, our observations indicate that calcium increase at synapses undergoing
591 sustained activity allows the transient recruitment of ALG-2, Alix and endophilin-A
592 sequentially to presynaptic parts. Because of the demonstrated roles of Alix in clathrin-
593 independent endocytosis, we next tested if the turnover of presynaptic vesicles might be
594 affected by the lack of the protein by quantifying Syp-pH fluorescence during electrical
595 stimulation. Syp-pH fluorescence increases during stimulation witnessing exocytosis. It decays
596 thereafter reflecting SV retrieval and vesicle re-acidification (Soykan et al., 2017). As shown in

597 **figures 3A and B**, no striking difference in the increase of fluorescence was detected between
598 Alix ko and wt neurons stimulated at 5 or 40 Hz. However, the time constant of the exponential
599 decay was slightly decreased in Alix ko neurons stimulated at 40 Hz, suggesting a higher rate
600 of Syp-pH endocytosis occurring at this frequency (**Figure 3B**).

601 We next tested if the proteins might intervene in activity-dependent bulk endocytosis
602 (ADBE) at synapses. Cultured cerebellar granular neurons (CGN) have been extensively used
603 to study this process (Cheung et al., 2010). Here, neurons were depolarized with 50 mM KCl,
604 in the presence of Horse Radish Peroxidase (HRP) that is endocytosed and fills vesicles and
605 endosomes as they form. Examination of wt synapses by electron microscopy showed that
606 depolarization dramatically increased the number of HRP-positive vacuoles. We verified using
607 FIB SEM and 3D reconstruction that these vacuoles had undergone fission from the plasma
608 membrane and could therefore be identified as bulk endosomes (**Figure 3C** yellow
609 arrowheads; **Figure 3D, E**). Other HRP-positive vesicles having the size of neurotransmitter
610 vesicles were also more numerous in depolarized synapses (**Figure 3C** blue arrowheads; **Figure**
611 **3D, E**). In Alix ko synapses, the number of depolarization-induced bulk endosomes was
612 strongly reduced (**Figure 3E, F**). Consistent with the increased endocytic rate detected by Syp-
613 pH in Alix ko neurons stimulated at 40 Hz (**Figure 3B**), the number of newly formed SV was
614 significantly increased, suggesting a mechanism compensating for ADBE deficiency (**Figure 3E,**
615 **G**).

616 Another way to assess for ADBE is by the use of fluorescent 10 kDa dextran, a fluid phase
617 cargo that accumulates inside bulk endosomes but fails to label vesicles formed by clathrin-
618 dependent mechanisms upon neuronal stimulation (Clayton and Cousin, 2009a). Hippocampal
619 neurons incorporated dextran when incubated in presence of bicuculline/4AP (**Figure 4A, B**).
620 A GSK3 inhibitor, known to block ADBE but no other modes of SV endocytosis (Clayton et al.,
621 2010), completely abolished the dextran labelling of wt hippocampal neurons
622 (**Supplementary figure 3A, B**). In contrast, Alix ko neurons failed to endocytose dextran
623 (**Figure 4A, B**) even though bicuculline/4AP stimulation increased calcium entry
624 (**Supplementary Figure 1A**) and neuronal activity (**Supplementary figure 3C-F**) in both Alix ko
625 and wt neurons. Noteworthy is that even though bicuculline/4AP increased activity in both
626 cases, the frequency of burst was significantly reduced in Alix ko neurons (**Supplementary**
627 **figure 3C, D**). As already shown (Morton et al., 2015), neurons also failed to endocytose
628 dextran when treated with calcium chelators BAPTA and EGTA (**Supplementary figure 3E**),

629 both of which blocked Alix recruitment to presynaptic boutons (**Supplementary figure 2**).
630 Finally, expression of GFP-Alix constructs in Alix ko neurons showed that the impairment in
631 ADBE observed in Alix ko cells is due solely to the absence of Alix, since Alix expression fully
632 restored the capacity of Alix ko neurons to endocytose 10 kDa dextran (**Figure 4 C, D**). Rescue
633 was also obtained with AlixΔ4B, a mutant unable to bind the ESCRT-III protein CHMP4B. This
634 was not the case with AlixΔALG-2 or AlixΔEndo which were not able to rescue dextran
635 endocytosis (**Figure 4D**). Noteworthy is that AlixΔALG-2 cannot be recruited to synapses but
636 both AlixΔendo and AlixΔ4B are. Thus, besides its requirement for ALG-2-binding to be
637 recruited at synapses, Alix needs to interact with endophilins but not with CHMP4B-ESCRT-III
638 in order to drive ADBE.
639
640 Synaptic anomalies detected in Alix ko mice
641 To study the effect of Alix deletion *in vivo*, we first compared brains of Alix ko (Laporte et
642 al., 2017) and wt mice and found that the density of synaptic contact as well as dendritic spines
643 in the CA1 hippocampal region of adult brains was not different (**Figure 5A, Supplementary**
644 **Figure 4**). This indicates that Alix is not required for synaptogenesis, a conclusion confirmed
645 *in vitro* since the number of synapses revealed by co-immunostaining with synapsin-1 and
646 PSD95 was similar between wt and Alix ko cultured hippocampal neurons (**Figure 5B**).
647 However, examination of the CA1 *stratum radiatum* of adult mice showed that Alix ko
648 synapses contained significantly fewer synaptic vesicles (SV) than wt (**Figure 5C, D**).
649 Furthermore, the size of postsynaptic densities, known to be strictly correlated with the
650 number of SV (Harris and Stevens, 1989), was similarly reduced in Alix ko synapses (**Figure 5F,**
651 **G**). Importantly, the surface of Alix ko synaptic boutons was also significantly increased
652 possibly suggesting plasma membrane accumulation in these synapses (**Figure 5C, E**). Finally,
653 at the postsynaptic level, we also noticed that the ratio between the diameter of the spine
654 head and that of the neck was changed in Alix ko animals, which can reflect defects in
655 maturation or plasticity of adult synapses (**Figure 5F, H**). Accordingly, field recordings in the
656 CA1 *stratum radiatum* of hippocampal slices revealed that long-term potentiation (LTP)
657 induced by tetanic stimulations was significantly impaired in Alix ko hippocampal slices
658 (**Supplementary Figure 5**).
659
660 Voltage-clamp recordings uncovers anomalies at Alix ko synapses.

661 In order to better characterize the effect of the lack of Alix on the physiology of synapses,
662 we next used Alix conditional-ko mice where Alix is deleted in neocortical and hippocampal
663 excitatory neurons (Gorski et al., 2002) (**Figure 6A**). We first recorded CA1 neurons of
664 hippocampal slices and found that the amplitude of spontaneous EPSCs was unaffected
665 whereas the frequency of events was significantly lower in Alix ko neurons (**Figure 6B, C**). This
666 was reminiscent of the reduced frequency of burst measured by MAE in dissociated
667 hippocampal cultures (**Supplementary figure 3C, D**). Stimulation of Schaffer collaterals
668 revealed that evoked EPSCs have a smaller amplitude in Alix ko brains than in wt animals
669 (**Figure 6D, E**). In order to estimate the amount of the readily releasable pool (RRP), we
670 performed repeated stimulations and integrated the EPSC amplitudes to give a cumulative
671 plot during 10 Hz trains. Linear regression fit to the last 10 data points was back extrapolated
672 to time 0 (dotted line) to estimate the cumulative EPSC before steady state depression. This
673 rough estimate of the RRP size (Schneggenburger et al., 1999) revealed that it is two times
674 smaller in Alix ko neurons (**Figure 6F**), in good agreement with the lower amounts of SVs
675 quantified in EM sections of synapses of the CA1 *stratum radiatum* (**Figure 5D**). Interestingly,
676 we could observe that the rate of recovery post-depression appears faster in Alix ko mice, a
677 possible mechanism of compensation for the reduced pool of synaptic vesicles (**Figure 6G, H,**
678 **I**).
679 Thus, these electrophysiological results show that synapses of Alix ko neurons which lack
680 ABDE have less SVs but increased rate of endocytosis, as already suggested in cultured
681 neurons by the increase of Syp-pH endocytosis and of newly formed SVs detected in Alix ko-
682 hippocampal and CB neurons, respectively.
683
684 <u>Alix conditional ko mice undergo less kainate induced acute seizures.</u>
685 We next examined the possible *in vivo* consequences of synaptic changes detected during
686 repeated stimulation of Alix ko neurons in hippocampal slices. Because of our earlier finding
687 of Alix increase at synapses of the rat hippocampus after kainaite injections (Hemming et al.,
688 2004) we tested how the lack of Alix might influence kainate induced epileptic seizures, a
689 mouse model for human temporal lobe epilepsy (Bedner et al., 2015). The unilateral
690 intracortical kainate injection induces the acute phase, *status epilepticus*, characterized by
691 high seizure frequency, during several hours. Seizure activity was determined by telemetric
692 EEG recording and synchronized video monitoring (**Figure 7A**). Here we used again the

693 conditional-ko mice where Alix is deleted in neocortical and hippocampal excitatory neurons
694 (**Figure 6A**). The total duration of *status epilepticus* (SE) was comparable in Alix ko and control
695 mice (**Figure 7B**). However, Alix cko mice experienced about 70 % less seizures than control
696 mice (**Figure 7C**). The average seizure duration was only minimally reduced in Alix ko
697 compared to control (**Figure 7D**). These results show that the absence of Alix selectively
698 reduces the number of high frequency events (single seizures), without affecting the total
699 duration of *status epilepticus*.
700 This kainate injection paradigm produces seizures originating from the hippocampus, which
701 can spread to other contralateral brain areas (Bedner et al., 2015). Microglial reactivity was
702 detected 24 h after kainate injection in ipsilateral and contralateral cortex and hippocampus
703 in both control and Alix cko animals (**Supplementary Figure 6A-E**). While the difference
704 between ipsi-and contralateral side was non-significant in control animals (≈ 10%), Alix ko
705 animals displayed a significantly reduced contralateral microglial activation (≈ 30%)
706 (**Supplementary Figure 6E**). No difference between Alix ko and control animals was detected
707 using GFAP immunolabelling, an expected result since astroglial activation peaks 4-7 days
708 after kainate injection (**Supplementary Figure 6F**). Thus, the reduced contralateral microglial
709 activation seen in Alix ko animals indicates a reduced propagation of the seizure activity and
710 corroborates the previous seizure quantification (**Figure 7C**).
711 In summary, Alix is specifically required for ADBE. Impairment in this process seems to
712 relate to impairments in synaptic function and plasticity in normal and pathological settings.
713

714 **Discussion**

715 To sustain neurotransmission and prevent expansion of the presynaptic plasma membrane,
716 synaptic vesicle (SV) fusion is coupled to the endocytic recycling and regeneration of SV
717 proteins and lipids. Vesicle components can be retrieved from the plasma membrane via
718 clathrin scaffolds, or via clathrin-independent processes mediating fast and ultrafast
719 endocytosis and, in the case of high frequency stimulation, bulk endocytosis (Gan and
720 Watanabe, 2018). Using Alix ko cells, we recently discovered that Alix drives clathrin-
721 independent-endocytosis (CIE) during ligand-induced endophilin-dependent endocytosis as
722 well as bulk endocytosis (Laporte et al., 2017; Mercier et al., 2016). We had previously
723 reported that Alix immunoreactivity in the rat hippocampus is strongly upregulated in
724 synapses undergoing high frequency activation during kainate-induced epileptic seizures. This
725 increase was presynaptic and only transient, as it was reversed soon after cessation of the
726 seizures (Hemming et al., 2004). The aim of the present study was to decipher the role of Alix
727 in endocytosis at synapses. We first used primary cultures of cortical and hippocampal
728 neurons, which make networks undergoing spontaneous activities. Massive increases in spike
729 frequency induced by 4AP and bicuculline resulted in elevated calcium entry (Hardingham et
730 al., 2001) and triggered activity dependent bulk endocytosis (ADBE) together with a transient
731 concentration of Alix at presynaptic parts. Quantifying bulk endocytosis using dextran uptake
732 or electron microscopy observations showed that ADBE is strongly reduced in Alix ko neurons
733 demonstrating that Alix is essential for ADBE. ADBE is triggered by high [Ca^{2+}] in response to
734 sustained activity (Paillart et al., 2003). Calcium and calmodulin-dependent phosphatase
735 calcineurin were suggested to make a link between synaptic activity and formation of bulk
736 endosomes through dynamin (Morton et al., 2015). Alix may represent another link as its
737 recruitment and activity in ADBE seems dependent on calcium increase. Indeed, EGTA, which
738 binds calcium at an approximately 100 times slower on-rate than BAPTA (Adler et al., 1991;
739 Schneggenburger and Neher, 2005), and was already known to block ADBE without affecting
740 synaptic release, was equally efficient as BAPTA in inhibiting Alix recruitment. Furthermore,
741 Alix recruitment required its capacity to bind the calcium-binding protein ALG-2, which also
742 concentrated at hyperactive synapses. ALG-2 is a cytosolic penta-EF hand-containing protein
743 with two Ca^{2+} binding sites (Kd= 1.2 μM), and its interaction with Alix strictly depends on
744 calcium (Missotten et al., 1999; Shibata et al., 2004; Trioulier et al., 2004). Conformational
745 change and exposure of hydrophobic patches occur at μM concentrations of Ca^{2+}, suggesting

746 that ALG-2 functions as a calcium sensor (Maki et al., 2016). Indeed, in non-neuronal cells,
747 calcium entry provoked by membrane wounds leads to the sequential recruitment to the
748 membrane of ALG-2, Alix and ESCRT-III proteins necessary for membrane repair (Jimenez et
749 al., 2014; Scheffer et al., 2014). In neurons, the activity-dependent accumulation of ALG-2 at
750 synapses required Ca^{2+} binding as it was totally abolished by point-mutations within the two
751 Ca^{2+} binding sites. On the other hand, it did not require Alix, as ALG-2 recruitment also
752 occurred in Alix ko neuron. Thus, our observations highlight synaptic ALG-2 as an obvious
753 candidate for sensing calcium elevation and suggest the following scenario: sustained high
754 frequency depolarization leads to massive elevation of calcium in the synaptic bouton; Ca^{2+}
755 binding to ALG-2 causes its accumulation at the synaptic membrane and binding to cytosolic
756 Alix, whose recruitment to the membrane drives ADBE.

757 Little is known about the molecular mechanisms underlying the plasma membrane
758 deformation during ADBE. The proline rich domain of Alix interacts with the SH3 domains of
759 endophilins-A1-3 which contain N-BAR domains and have been shown to regulate clathrin-
760 dependent and -independent SV endocytosis at different synapses (Gad et al., 2000; Llobet et
761 al., 2011; Ringstad et al., 1999). BAR domains are dimerization domains able to induce,
762 stabilize and sense membrane curvature (Farsad et al., 2001; Kjaerulff et al., 2011).
763 Interestingly, a proteomic approach revealed the presence of endophilin-A1, Alix and ALG-2
764 in bulk endosomes (Kokotos et al., 2018). Furthermore, endophilin-A2, actin and dynamin
765 mediate a restricted type of CIE activated upon ligand binding to cargo receptors (Boucrot et
766 al., 2014; Renard et al., 2014). We previously showed that in fibroblasts, endophilin-A and Alix
767 act in the same CIE pathway, even if Alix is more promiscuous for ligands, as it is also involved
768 in fluid phase endocytosis. In this case interaction of Alix with endophilins favoured their
769 presence at the membrane (Mercier et al., 2016). We now found that endophilin-A2
770 decorated presynapses of resting neurons and that Alix was needed for its synaptic
771 enrichment during stimulation. An Alix point mutant unable to interact with endophilin was
772 recruited to synapses but could not rescue ABDE in Alix ko neurons, reminiscent of the
773 situation seen in fibroblasts (Mercier et al., 2016). Thus, a complex between endophilin-A and
774 Alix is required for ADBE. One function of Alix might be to enable endophilin-A binding onto
775 flat membranes of the peri-active zone to drive membrane bending in response to high
776 calcium concentrations (Boucrot et al., 2014; Kjaerulff et al., 2011). Interestingly, the
777 incapacity of Alix to interact with Chmp4B from ESCRT-III, known to alleviate its plasma

778 membrane repair ability (Jimenez et al., 2014; Scheffer et al., 2014), did not alter rescue of
779 ADBE. This result also discriminates Alix-driven ADBE from roles of the ESCRT system in the
780 degradation of SV proteins (Sadoul et al., 2017; Sheehan et al., 2016).
781 Electrophysiological recordings and EM observations in CA3-CA1 synapses both point to a
782 reduction in the number of synaptic vesicles due to the lack of Alix and possibly to the
783 associated defects in ADBE. On the other hand, Syp-pH fluorescence and EM analysis
784 revealed that activity dependent synaptic endocytosis is increased in absence of Alix.
785 Accordingly, electrophysiological patch-clamp recordings show that Alix ko CA3-CA1 synapses
786 recover better from STD induced by repeated stimulations Thus, compensation by increased
787 endocytosis, is not sufficient to rescue the phenotype. This could be a first demonstration that
788 ADBE of the essential role of ADBE in regulating the number of synaptic vesicles and thereby
789 normal synaptic function.
790 Excitatory, glutamatergic neurotransmission plays a central role in the generation of seizure
791 activity (Albrecht and Zielińska, 2017; Barker-Haliski and White, 2015) and figures among the
792 primary anti-epileptic drug targets (Rogawski and Löscher, 2004). Sustained, intense and
793 synchronous neurotransmission as occurring during seizures requires replenishment of
794 synaptic vesicle pools mainly through activity-dependent bulk endocytosis (ADBE) (Cheung
795 and Cousin, 2012). Impairing ADBE *in vivo,* by deleting Alix in neocortical and hippocampal
796 excitatory neurons led to a significantly reduced number of seizures during SE, without
797 affecting the total duration of SE or the mean seizure duration. The present results suggest
798 that excitatory networks lacking Alix have a reduced capacity to initiate sequential seizures,
799 possibly due to an impaired replenishment of synaptic vesicles through ADBE. Seizure
800 termination and *status epilepticus* cessation however seem to be governed by distinct
801 mechanisms, probably involving inhibitory transmission to re-establish the balance between
802 excitation and inhibition in the brain. Our results highlight Alix ko mice as an invaluable tool
803 for exploring and understanding the exact role of ADBE at synapses undergoing normal and
804 pathological stimulations.
805

Acknowledgements

We thank J. Brocard for helping with data analysis, Y. Saoudi for helping with fluorescence microscopy, N. Liaudet from the Bioimaging core facility of the University of Geneva for his help with the segmentation and electron microscopy, F. Saudou for making the MEA experiments possible. We also thank K. Sadoul for critically reading the manuscript. This work was funded by France Alzheimer (R.S.), Ministère de l'Enseignement Supérieur et de la Recherche (K.I.C, M.R. and M.H.L.), Marie Sklodowska-Curie post-doctoral fellowship (M.M.); EC H2020 MSCA-ITN EU-GliapHD #722053 (L.C.C. and F.K.), Agence Nationale de la Recherche ANR (J.M.-H.) and Fondation pour la Recherche Medical FRM (E.M.).

Competing interests

On behalf of all authors, R.Sadoul declares no competing interests.

Author contributions

RS conceived the project. MHL participated to most of the in vitro experiments and analysed electron microscopy data under the supervision of SF. KIC performed and analysed most of the *in vitro* experiments concerning live imaging of Alix recruitment and dextran uptake. LCC performed and analysed the EEG telemetry and unilateral intracortical kainate injection. NZ performed and analysed patch clamp electrophysiological recordings. The experiments of LCC and NZ were done under the supervision of FK. MR and FLa performed field electrophysiological recordings. JM-H performed electron microscopy of mouse brains. MM and DP performed and analysed the live imaging of synaptophysin-pHluorin during electrical stimulation. CC performed mouse breeding, genotyping and participated in *in vitro* experiments. ED helped with data analysis of live imaging. VM performed FIB-SEM imaging. BB performed mouse genotyping and construction of plasmids. EM and MC performed and analysed multielectrode array experiments. FLe did some of the live imaging experiments of Alix recruitment *in vitro*. FJH performed electron microscopy of cultured neurons. RS and MHL wrote the manuscript with input from all other authors.

835 **Figure legends**
836
837 **Figure 1. Alix is recruited presynaptically during synaptic activation. A**) Western blot analysis of
838 cortical neurons cultured for 3 to 15 DIV demonstrates the increase in Alix expression correlating with
839 synaptogenesis as illustrated by the increase in PSD95 expression. **B**) Western blot analysis of the
840 increase of Alix in synaptosome-enriched neuronal membranes upon neuronal stimulation by
841 bicuculline/4AP. Synaptophysin and PSD95 were used as pre- and postsynaptic markers, respectively.
842 The phosphorylated form of ERK (p-ERK) assessed the efficiency of the stimulation. **C**) Images from
843 time-lapse video microscopy of 15 DIV hippocampal neurons expressing both mCherry-Alix (mche-Alix)
844 and synaptophysin-pHluorin (Syp-pH) stimulated between 2 and 7 minutes with bicuculline/4AP.
845 White arrowheads indicate presynaptic boutons where Alix is recruited during stimulation. Scale bar:
846 10 µm. **D**) Profiles of mcherry-Alix and Syp-pH fluorescent increase at presynaptic boutons 1 and 2 of
847 panel **C**. Blue box indicates the bicuculline/4AP stimulation. **E**) 15 DIV hippocampal neurons expressing
848 Alix-YFP (green) stimulated for 5 min before fixation and stained with anti-synapsin-1 antibody (Syn,
849 magenta). Scale bar: 5 µm. **F**) Graph shows the presynaptic increase in Alix-YFP upon stimulation.
850 Presynaptic Alix-YFP corresponds to the ratio of YFP fluorescence between synapsin-positive and -
851 negative axonal regions. **G**) 15 DIV hippocampal neurons expressing Alix-YFP (green) stimulated for 5
852 min before fixation and stained with anti-synapsin-1 antibody (Syn, magenta) and anti-PSD95 (post-
853 synaptic, cyan) showing the selective recruitment of Alix to presynpase. Scale bar: 5 µm.
854 Average +/- SEM, N, statistical analysis: **B)** 2.07+/-0.34; 1.38+/-0.21; 1.00+/-0.01 for Alix,
855 Synaptophysin and PSD95 respectively. N=4 independent experiments, Alix versus PSD95, p=0.0187,
856 one-way ANOVA. **F**) 1.63+/-0.12; 3.27+/-0.44 for No Stim and Stim respectively. N=12 neurons per
857 condition from 4 independent experiments, p=0.0017, Unpaired t-test.
858
859 **Figure 2. Interplay between Alix, ALG-2 and endophilin recruitments at activated synapses.** All
860 experiments made use of 15 DIV hippocampal neurons expressing the indicated constructs. Neurons
861 were stimulated with bicuculline/4AP for 5 min before fixation and stained with anti-synapsin-1 (Syn,
862 magenta). **A**) GFP-ALG-2 (green) is recruited presynaptically upon stimulation. Scale bar: 5 µm. **B**)
863 Quantification of synaptic recruitments of GFP-ALG-2 and GFP-ALG-2ΔCa in Alix wt neurons shows that
864 ALG-2 presynaptic increase depends on its capacity to bind calcium. **C**) Alix recruitment depends on its
865 capacity to bind ALG-2 as GFP-AlixΔALG-2 is not recruited upon stimulation of Alix ko neurons.
866 However, ALG-2 does not require Alix to be recruited as GFP-ALG-2 is recruited presynaptically in Alix
867 ko neurons. **D**, **E**) Endophilin-mCherry (endo, green) concentrates at presynaptic parts of stimulated
868 neurons. Scale bar: 5 µm. **F**) Endophilin concentration following synaptic activation requires Alix as it
869 does not occur in Alix ko neurons. Alix recruitment does not depend on its binding to endophilins as
870 shown with GFP-AlixΔendo in Alix ko neurons.
871 Average +/- SEM, N, statistical analysis: **B)** 1.41+/-0.13; 2.24+/-0.11; 1.38+/-0.05; 1.18+/-0.15 for GFP-
872 ALG-2 no stim, GFP-ALG-2 stim, GFP-ALG-2ΔCa no stim, GFP-ALG-2ΔCa stim respectively. N=7 and n=10
873 neurons for GFP-ALG-2 not stimulated and stimulated, respectively and n=12 and n=6 neurons for GFP-
874 ALG-2ΔCa not stimulated and stimulated, respectively, from 3 experiments, p=0.0001, one-way
875 ANOVA. **C)** 1.37+/-0.07; 2.06+/-0.11; 1.54+/-0.05; 1.48+/-0.08 for GFP-ALG-2 no stim; GFP-ALG-2 stim,
876 GFP-AlixΔALG-2 no stim, GFP-AlixΔALG-2 stim respectively. N=17 neurons for both GFP-ALG-2 not
877 stimulated and stimulated, and n=18 and n=15 neurons for GFP-AlixΔALG-2 not stimulated and
878 stimulated, respectively, from 3 independent experiments, p=0.0001, one-way ANOVA. **D,E)** 1.92+/-
879 0.11; 3.48+/-0.33 for no stim and stim respectively. N=10 and n=12 neurons for not stimulated and
880 stimulated, respectively from 3 independent experiments, p=0.0001, Mann Whitney test. **F)** 2.37+/-
881 0.12; 2.66+/-0.08; 1.56+/-0.06; 2.43+/-0.32 for endophilin-mCherry no stim, endophilin-mCherry stim,
882 GFP-AlixΔendo no stim, GFP-AlixΔendo stim respectively. N=13 and n=15 neurons for endophilin-
883 mCherry not stimulated and stimulated, respectively, and n=10 and n=9 neurons for GFP-AlixΔendo
884 not stimulated and stimulated, respectively, from 3 independent experiments p=0.0031, one-way
885 ANOVA.
886

887
888 **Figure 3. Alix is necessary for activity-dependent bulk endocytosis. A**, **B**) Average traces of Syp-pH
889 fluorescence in synaptic boutons of Alix wt and ko hippocampal neurons stimulated with 200 action
890 potentials (AP) applied at 5 Hz (**A**) or 40 Hz (**B**). Insets show the exponential fit of fluorescence decay
891 after stimulations in the fields imaged. **C**, **E**) Electron micrographs of cerebellar granule neurons
892 stimulated in presence of free HRP to label newly-formed synaptic vesicle (blue arrowhead) and bulk
893 endosomes (yellow arrowheads). **C**) Focused ion beam scanning electron microscopy (FIB-SEM);
894 orthogonal views from different planes (xy, xz, yz) extracted from a stack used for the 3D
895 reconstruction of wt presynaptic terminal shown in (**D**). Scale bar: 500nm. **D**) Two different views of
896 the reconstructed synapse are shown where the membrane is represented in transparent gray and
897 HRP-positive structures in red. Scale bar: 500nm. E) Transmission electron microscopy of HRP
898 incubated CB Alix wt and Alix ko neurons. Scale bar: 100 nm. **F**, **G**) Quantification of the number of bulk
899 endosomes (**F**) and synaptic vesicles (**G**) in Alix wt and ko neurons from images as shown in (E).
900 Average +/- SEM, N, statistical analysis: **A**, **B**) N= 16-46 fields of view per condition from 4 experiments
901 for wt and 5 for ko mice, p=0.99 (**A**) and p=0.001 (**B**), one-way ANOVA. **F**, **G**) 0.52+/-0.17; 0.64+/-0.15;
902 3.28+/-0.19; 1.82+/-0.06 for Alix wt no stim, Alix ko no stim, Alix wt stim, Alix ko stim respectively (**F**).
903 4.43+/-1.02; 4.26+/-0.58; 7.46+/-0.49; 9.64+/-0.67 for Alix wt no stim, Alix ko no stim, Alix wt stim, Alix
904 ko stim respectively (**G**). N= 44 and 51 neurons from 4 independent experiments, p<0.0001 (Alix wt no
905 stim vs Alix wt stim, **F**), p=0.0015 (Alix ko no stim vs Alix ko stim, **F**), p=0.0001 (Alix wt stim vs Alix ko
906 stim, **F**) and p=0.0376 (Alix wt no stim vs Alix wt stim, **G**), p=0.0014 (Alix ko no stim vs Alix ko stim, **G**),
907 p=0.0393 (Alix wt stim vs Alix ko stim, **G**), one-way ANOVA.
908
909 **Figure 4. Alix-driven bulk endocytosis requires its binding to ALG-2 and endophilin but not to CHMP4.**
910 **A**) Confocal images of Alix wt and Alix ko hippocampal neurons stimulated with Bicucculine/4AP in the
911 presence of 10kDa dextran. Scale bar: 50 µm. **B**) Dextran uptake triggered by stimulation is strongly
912 reduced in Alix ko neurons. **C**) Representative images of Dextran uptake by GFP-expressing Alix wt and
913 Alix ko neurons (Alix wt, top and Alix ko,middle) or Alix ko neurons expressing both GFP and Alix (Alix
914 ko+Alix, bottom). Scale bars: 10 µm. **D**) Dextran uptake is rescued in ko neurons expressing Alix wt and
915 AlixΔChmp4B (AlixΔ4B), but not AlixΔALG-2 or AlixΔendo. % of dextran uptake corresponds to the
916 number of dextran spots per µm expressed as percentages of the control (Alix wt) for each experiment.
917 Average +/- SEM, N, statistical analysis: **B)** 16.26+/-1.08; 11.86+/-2.05; 100+/-1.76; 15.10+/-1.76 for
918 Alix wt no stim, Alix ko no stim, Alix wt stim, Alix ko stim respectively. N=4 experiments, p=0.0001, one-
919 way ANOVA. **D)** 100+/-6.31; 33.27+/-3.32; 94.78+/-5.81; 45.89+/-9.36; 80.05+/-7.32; 44.59+/-1.85
920 for Alix wt, Alix ko, Alix ko + Alix, Alix ko + AlixΔChmp4B, Alix ko + AlixΔendo, Alix ko + AlixΔALG-2. N=17
921 neurons for Alix wt, n=13 neurons for Alix ko, n=11 for Alix ko + Alix, n=12 for Alix ko + AlixΔChmp4B,
922 n=12 neurons for Alix ko + AlixΔendo, , and n=11 for Alix ko + AlixΔALG-2, all from 3-4 independent
923 experiments, p=0.62 (Alix wt vs Alix AlixΔ4B) p=0.0001 for the other conditions, one-way ANOVA).
924
925 **Figure 5. Morphological anomalies of Alix ko synapses. A**) Representative electron micrographs of the
926 CA1 stratum radiatum from Alix wt and ko brain sections. Presynaptic profiles are highlighted in blue,
927 and dendritic spines are in purple. Scale bar: 2 µm. Graph shows no difference in synaptic density per
928 μm^2 of Alix wt and ko brains. **B**) 15 DIV hippocampal neurons were stained with anti-PSD95 (magenta)
929 and anti-synapsin-1 (green) antibodies. Immunolabelled objects were considered as synapses when
930 both stainings were juxtaposed. Scale bar: 10 µm. Graph shows no difference in the number of
931 synapses per μm^2 of Alix wt and ko neurons). **C-H**) Anomalies can be detected in synapses of Alix ko
932 brains. **C**, **F**) Representative electron micrographs of CA1 from Alix wt and ko mice. Scale bar: 200 nm.
933 Graphs represent the numbers of synaptic vesicles per μm^2 (**D**), presynaptic bouton surface area (**E**),
934 PSD length (**F**), ratio between the diameter of the spine head and neck (**G**).
935 Average +/- SEM, N, statistical analysis: **A)** 0.40+/-0.02; 0.45+/-0.03 for Alix wt and Alix ko respectively.
936 N=600 synapses from 3 animals per genotype, p=0.1395, Unpaired t-test. **B)** 0.13+/-0.01; 0.12+/-0.01
937 for Alix wt and ko respectively. N=7 independent experiments, p=0.5501, Unpaired t-test.

938 Median (min to max), N, statistical analysis **D**) 165.4 (69 to 278); 127.3 (31 to 336) for Alix wt and Alix
939 ko respectively. N=136 synapses from 3 animals, p=0.0009, Mann Whitney test). **E)** 0.13 (0.027 to
940 0.376); 0.16 (0.053 to 0.47) for Alix wt and Alix ko respectively. N=136 synapses from 3 animals,
941 p=0.0036, Mann Whitney test). **G)**: 0.76 (0.25 to 1.48) ; 0.54 (0.13 to 1.11) for Alix wt and Alix ko
942 respectively. N=136 synapses from 3 animals, p=0.0001, Mann Whitney test). **H)** 2.58 (0.85 to 5.60);
943 1.68 (0.58 to 4.78) for Alix wt and Alix ko respectively. N=136 synapses from 3 animals, p=0.0001, Mann
944 Whitney test.
945

946 **Figure 6. Voltage-clamp recordings uncover anomalies at Alix ko synapses**. **A**) Emx1 ^{IREScre} (Emx-Cre)
947 and Alix $^{fl/fl}$ mouse lines were crossbred to delete Alix in neocortical and hippocampal excitatory
948 neurons (Alix cko). **B**) No difference in spontaneous Excitatory Post Synaptic Current (sEPSC) amplitude
949 was detected between control and cko mice. **C**) The frequency of sEPSC in cko neurons is lower
950 compared to control. **D**) Representative traces showing short-term depression in response to 10 Hz
951 stimulation trains in control (black) and cko (grey) mice. **E**) Cumulative EPSC amplitudes in response to
952 10 Hz stimulation. Train-extrapolation is illustrated by the dashed line. **F**) The size of the readily
953 releasable pool, estimated by the train-extrapolation method, was significantly decreased in Alix cko
954 mice. **G**) Representative traces showing recovery from depression in response to 10 Hz stimulation
955 trains in control (black) and Alix cko (grey) mice. **H**) To evaluate the speed of recovery, all inward signals
956 were normalized to 1st inward current. Recovering signals with a single-exponential function revealed
957 the plateaus at which the capacities of recovery were saturated. **I**) Alix cko neurons slightly recover
958 faster than controls.
959 Average +/- SEM, N, statistical analysis: **B)** 9.79+/-0.53; 8.88+/-0.42 for controls and Alix cko
960 respectively. N=11 neurons from 5 control mice and N=17 neurons from 6 Alix cko mice, p=0.1875,
961 unpaired t test. **C)** 0.93+/-0.25; 0.44+/-0.10 for controls and Alix cko respectively. N=11 neurons from
962 5 control mice and N=17 neurons from 6 Alix cko mice, **p=0.0095, Mann Whitney test. **F)** 1.23+/-
963 0.15; 0.67+/-0:08 for controls and Alix cko respectively. N=12 neurons from 5 control mice, and N=10
964 neurons from 4 Alix cko mice, **p=0.0052, unpaired t test. **I)** 8.34+/-0.90; 5.56+/-0.69 for controls and
965 Alix cko respectively. N= 5 and 6 neurons from 3 mice from control and Alix cko respectively,
966 *p=0.0336, unpaired t test.
967

968 **Figure 7. Alix cko mice develop less seizures during status epilepticus. A**) Representative EEG traces
969 from control and Alix cko mice. **B**) Total duration of *status epilepticus* (SE) did not differ between Alix
970 cko and control mice. **C**) Alix cko mice experience about 66 % less seizures during SE than controls. **D**)
971 Mean seizure duration during SE was not affected in Alix cko mice compared to controls.
972 Median + IQR, N, statistical analysis: **A**, **B**) 1.6 h (IQR = 2.5); 1.7 h (IQR = 0.9) for control and Alix cko
973 mice respectively. N=11 mice for both genotype, p= 0.49, Mann-Whitney test. **C**) 18 seizures (IQR = 9);
974 8 seizures (IQR = 9) for control and Alix cko mice respectively. N=11 mice for both genotypes, *p= 0.03,
975 Mann-Whitney test. **D**) 32.9 s (IQR = 18.6); 25.7 h (IQR = 12.7) for control and Alix cko mice
976 respectively. N=11 mice for both genotype, p= 0.19, Mann-Whitney test.
977
978
979

980 **References**

981 Adler, E.M., Augustine, G.J., Duffy, S.N., and Charlton, M.P. (1991). Alien intracellular calcium
982 chelators attenuate neurotransmitter release at the squid giant synapse. J Neurosci *11*,
983 1496-1507.
984 Albrecht, J., and Zielińska, M. (2017). Mechanisms of Excessive Extracellular Glutamate
985 Accumulation in Temporal Lobe Epilepsy. Neurochem Res *42*, 1724-1734.
986 Barker-Haliski, M., and White, H.S. (2015). Glutamatergic Mechanisms Associated with
987 Seizures and Epilepsy. Cold Spring Harb Perspect Med *5*, a022863.

988 Bedner, P., Dupper, A., Huttmann, K., Muller, J., Herde, M.K., Dublin, P., Deshpande, T.,
989 Schramm, J., Haussler, U., Haas, C.A.*, et al.* (2015). Astrocyte uncoupling as a cause of human
990 temporal lobe epilepsy. Brain *138*, 1208-1222.
991 Bissig, C., Lenoir, M., Velluz, M.C., Kufareva, I., Abagyan, R., Overduin, M., and Gruenberg, J.
992 (2013). Viral infection controlled by a calcium-dependent lipid-binding module in ALIX. Dev
993 Cell *25*, 364-373.
994 Boucrot, E., Ferreira, A.P., Almeida-Souza, L., Debard, S., Vallis, Y., Howard, G., Bertot, L.,
995 Sauvonnet, N., and McMahon, H.T. (2014). Endophilin marks and controls a clathrin-
996 independent endocytic pathway. Nature.
997 Campos, Y., Qiu, X., Gomero, E., Wakefield, R., Horner, L., Brutkowski, W., Han, Y.G., Solecki,
998 D., Frase, S., Bongiovanni, A.*, et al.* (2016). Alix-mediated assembly of the actomyosin-tight
999 junction polarity complex preserves epithelial polarity and epithelial barrier. Nature
1000 communications *7*, 11876.
1001 Chanaday, N.L., and Kavalali, E.T. (2018). Time course and temperature dependence of
1002 synaptic vesicle endocytosis. FEBS Lett *592*, 3606-3614.
1003 Chassefeyre, R., Martinez-Hernandez, J., Bertaso, F., Bouquier, N., Blot, B., Laporte, M.,
1004 Fraboulet, S., Coute, Y., Devoy, A., Isaacs, A.M.*, et al.* (2015). Regulation of Postsynaptic
1005 Function by the Dementia-Related ESCRT-III Subunit CHMP2B. J Neurosci *35*, 3155-3173.
1006 Chatellard-Causse, C., Blot, B., Cristina, N., Torch, S., Missotten, M., and Sadoul, R. (2002).
1007 Alix (ALG-2-interacting protein X), a protein involved in apoptosis, binds to endophilins and
1008 induces cytoplasmic vacuolization. J Biol Chem *277*, 29108-29115.
1009 Cheung, G., and Cousin, M.A. (2012). Adaptor protein complexes 1 and 3 are essential for
1010 generation of synaptic vesicles from activity-dependent bulk endosomes. J Neurosci *32*,
1011 6014-6023.
1012 Cheung, G., Jupp, O.J., and Cousin, M.A. (2010). Activity-dependent bulk endocytosis and
1013 clathrin-dependent endocytosis replenish specific synaptic vesicle pools in central nerve
1014 terminals. J Neurosci *30*, 8151-8161.
1015 Clayton, E.L., and Cousin, M.A. (2009a). The molecular physiology of activity-dependent bulk
1016 endocytosis of synaptic vesicles. J Neurochem *111*, 901-914.
1017 Clayton, E.L., and Cousin, M.A. (2009b). Quantitative monitoring of activity-dependent bulk
1018 endocytosis of synaptic vesicle membrane by fluorescent dextran imaging. J Neurosci
1019 Methods *185*, 76-81.
1020 Clayton, E.L., Sue, N., Smillie, K.J., O'Leary, T., Bache, N., Cheung, G., Cole, A.R., Wyllie, D.J.,
1021 Sutherland, C., Robinson, P.J.*, et al.* (2010). Dynamin I phosphorylation by GSK3 controls
1022 activity-dependent bulk endocytosis of synaptic vesicles. Nat Neurosci *13*, 845-851.
1023 de Chaumont, F., Dallongeville, S., Chenouard, N., Herve, N., Pop, S., Provoost, T., Meas-
1024 Yedid, V., Pankajakshan, P., Lecomte, T., Le Montagner, Y.*, et al.* (2012). Icy: an open
1025 bioimage informatics platform for extended reproducible research. Nature methods *9*, 690-
1026 696.
1027 Farsad, K., Ringstad, N., Takei, K., Floyd, S.R., Rose, K., and De Camilli, P. (2001). Generation
1028 of high curvature membranes mediated by direct endophilin bilayer interactions. J Cell Biol
1029 *155*, 193-200.
1030 Faure, J., Lachenal, G., Court, M., Hirrlinger, J., Chatellard-Causse, C., Blot, B., Grange, J.,
1031 Schoehn, G., Goldberg, Y., Boyer, V.*, et al.* (2006). Exosomes are released by cultured cortical
1032 neurones. Mol Cell Neurosci *31*, 642-648.

1033 Frandemiche, M.L., De Seranno, S., Rush, T., Borel, E., Elie, A., Arnal, I., Lante, F., and
1034 Buisson, A. (2014). Activity-dependent tau protein translocation to excitatory synapse is
1035 disrupted by exposure to amyloid-beta oligomers. J Neurosci *34*, 6084-6097.
1036 Gad, H., Ringstad, N., Low, P., Kjaerulff, O., Gustafsson, J., Wenk, M., Di Paolo, G., Nemoto,
1037 Y., Crun, J., Ellisman, M.H.*, et al.* (2000). Fission and uncoating of synaptic clathrin-coated
1038 vesicles are perturbed by disruption of interactions with the SH3 domain of endophilin.
1039 Neuron *27*, 301-312.
1040 Gan, Q., and Watanabe, S. (2018). Synaptic Vesicle Endocytosis in Different Model Systems.
1041 Frontiers in cellular neuroscience *12*, 171.
1042 Gorski, J.A., Talley, T., Qiu, M., Puelles, L., Rubenstein, J.L., and Jones, K.R. (2002). Cortical
1043 excitatory neurons and glia, but not GABAergic neurons, are produced in the Emx1-
1044 expressing lineage. J Neurosci *22*, 6309-6314.
1045 Granseth, B., Odermatt, B., Royle, S.J., and Lagnado, L. (2006). Clathrin-mediated
1046 endocytosis is the dominant mechanism of vesicle retrieval at hippocampal synapses.
1047 Neuron *51*, 773-786.
1048 Hardingham, G.E., Arnold, F.J., and Bading, H. (2001). Nuclear calcium signaling controls
1049 CREB-mediated gene expression triggered by synaptic activity. Nat Neurosci *4*, 261-267.
1050 Hardingham, G.E., Fukunaga, Y., and Bading, H. (2002). Extrasynaptic NMDARs oppose
1051 synaptic NMDARs by triggering CREB shut-off and cell death pathways. Nat Neurosci *5*, 405-
1052 414.
1053 Harris, K.M., and Stevens, J.K. (1989). Dendritic Spines of Ca-1 Pyramidal Cells in the Rat
1054 Hippocampus - Serial Electron-Microscopy with Reference to Their Biophysical
1055 Characteristics. Journal of Neuroscience *9*, 2982-2997.
1056 Hemming, F.J., Fraboulet, S., Blot, B., and Sadoul, R. (2004). Early increase of apoptosis-
1057 linked gene-2 interacting protein X in areas of kainate-induced neurodegeneration.
1058 Neuroscience *123*, 887-895.
1059 Jimenez, A.J., Maiuri, P., Lafaurie-Janvore, J., Divoux, S., Piel, M., and Perez, F. (2014). ESCRT
1060 machinery is required for plasma membrane repair. Science *343*, 1247136.
1061 Kjaerulff, O., Brodin, L., and Jung, A. (2011). The structure and function of endophilin
1062 proteins. Cell biochemistry and biophysics *60*, 137-154.
1063 Kokotos, A.C., Peltier, J., Davenport, E.C., Trost, M., and Cousin, M.A. (2018). Activity-
1064 dependent bulk endocytosis proteome reveals a key presynaptic role for the monomeric
1065 GTPase Rab11. Proc Natl Acad Sci U S A *115*, E10177-E10186.
1066 Kononenko, N.L., Puchkov, D., Classen, G.A., Walter, A.M., Pechstein, A., Sawade, L., Kaempf,
1067 N., Trimbuch, T., Lorenz, D., Rosenmund, C.*, et al.* (2014). Clathrin/AP-2 mediate synaptic
1068 vesicle reformation from endosome-like vacuoles but are not essential for membrane
1069 retrieval at central synapses. Neuron *82*, 981-988.
1070 Körber, C., Horstmann, H., Venkataramani, V., Herrmannsdörfer, F., Kremer, T., Kaiser, M.,
1071 Schwenger, Darius B., Ahmed, S., Dean, C., Dresbach, T.*, et al.* (2015). Modulation of
1072 Presynaptic Release Probability by the Vertebrate-Specific Protein Mover. Neuron *87*, 521-
1073 533.
1074 Lagache, T., Grassart, A., Dallongeville, S., Faklaris, O., Sauvonnet, N., Dufour, A., Danglot, L.,
1075 and Olivo-Marin, J.C. (2018). Mapping molecular assemblies with fluorescence microscopy
1076 and object-based spatial statistics. Nature communications *9*, 698.
1077 Laporte, M.H., Chatellard, C., Vauchez, V., Hemming, F.J., Deloulme, J.C., Vossier, F., Blot, B.,
1078 Fraboulet, S., and Sadoul, R. (2017). Alix is required during development for normal growth
1079 of the mouse brain. Sci Rep *7*, 44767.

1080 Lidierth, M. (2009). sigTOOL: A MATLAB-based environment for sharing laboratory-
1081 developed software to analyze biological signals. J Neurosci Methods *178*, 188-196.
1082 Llobet, A., Gallop, J.L., Burden, J.J., Camdere, G., Chandra, P., Vallis, Y., Hopkins, C.R.,
1083 Lagnado, L., and McMahon, H.T. (2011). Endophilin drives the fast mode of vesicle retrieval
1084 in a ribbon synapse. J Neurosci *31*, 8512-8519.
1085 Maki, M., Takahara, T., and Shibata, H. (2016). Multifaceted Roles of ALG-2 in Ca(2+)-
1086 Regulated Membrane Trafficking. Int J Mol Sci *17*.
1087 Martineau, M., Somasundaram, A., Grimm, J.B., Gruber, T.D., Choquet, D., Taraska, J.W.,
1088 Lavis, L.D., and Perrais, D. (2017). Semisynthetic fluorescent pH sensors for imaging
1089 exocytosis and endocytosis. Nature communications *8*.
1090 Marxen, M., Volknandt, W., and Zimmermann, H. (1999). Endocytic vacuoles formed
1091 following a short pulse of K+ -stimulation contain a plethora of presynaptic membrane
1092 proteins. Neuroscience *94*, 985-996.
1093 Mercier, V., Laporte, M.H., Destaing, O., Blot, B., Blouin, C.M., Pernet-Gallay, K., Chatellard,
1094 C., Saoudi, Y., Albiges-Rizo, C., Lamaze, C.*, et al.* (2016). ALG-2 interacting protein-X (Alix) is
1095 essential for clathrin-independent endocytosis and signaling. Sci Rep *6*, 26986.
1096 Miller, T.M., and Heuser, J.E. (1984). Endocytosis of synaptic vesicle membrane at the frog
1097 neuromuscular junction. J Cell Biol *98*, 685-698.
1098 Milosevic, I., Giovedi, S., Lou, X., Raimondi, A., Collesi, C., Shen, H., Paradise, S., O'Toole, E.,
1099 Ferguson, S., Cremona, O.*, et al.* (2011). Recruitment of endophilin to clathrin-coated pit
1100 necks is required for efficient vesicle uncoating after fission. Neuron *72*, 587-601.
1101 Missotten, M., Nichols, A., Rieger, K., and Sadoul, R. (1999). Alix, a novel mouse protein
1102 undergoing calcium-dependent interaction with the apoptosis-linked-gene 2 (ALG-2) protein.
1103 Cell Death Differ *6*, 124-129.
1104 Morton, A., Marland, J.R., and Cousin, M.A. (2015). Synaptic vesicle exocytosis and increased
1105 cytosolic calcium are both necessary but not sufficient for activity-dependent bulk
1106 endocytosis. J Neurochem *134*, 405-415.
1107 Neher, E. (2015). Merits and Limitations of Vesicle Pool Models in View of Heterogeneous
1108 Populations of Synaptic Vesicles. Neuron *87*, 1131-1142.
1109 Paillart, C., Li, J., Matthews, G., and Sterling, P. (2003). Endocytosis and vesicle recycling at a
1110 ribbon synapse. J Neurosci *23*, 4092-4099.
1111 Racine, R.J. (1972). Modification of seizure activity by electrical stimulation. II. Motor
1112 seizure. Electroencephalogr Clin Neurophysiol *32*, 281-294.
1113 Renard, H., Simunovic, M., Lemiere, J., Boucrot, E., Garcia-Castillo, M.D., Arumugam, S.,
1114 Chambon, V., Lamaze, C., Wunder, C., Kenworthy, A.K.*, et al.* (2014). Endophilin-A2 functions
1115 in membrane scission in clathrin-independent endocytosis. Nature.
1116 Ringstad, N., Gad, H., Low, P., Di Paolo, G., Brodin, L., Shupliakov, O., and De Camilli, P.
1117 (1999). Endophilin/SH3p4 is required for the transition from early to late stages in clathrin-
1118 mediated synaptic vesicle endocytosis. Neuron *24*, 143-154.
1119 Rogawski, M.A., and Löscher, W. (2004). The neurobiology of antiepileptic drugs. Nat Rev
1120 Neurosci *5*, 553-564.
1121 Sadoul, R. (2006). Do Alix and ALG-2 really control endosomes for better or for worse. Bio
1122 Cell *98*, 69-77.
1123 Sadoul, R., Laporte, M.H., Chassefeyre, R., Chi, K.I., Goldberg, Y., Chatellard, C., Hemming,
1124 F.J., and Fraboulet, S. (2017). The role of ESCRT during development and functioning of the
1125 nervous system. Semin Cell Dev Biol.

1126 Scheffer, L.L., Sreetama, S.C., Sharma, N., Medikayala, S., Brown, K.J., Defour, A., and Jaiswal,
1127 J.K. (2014). Mechanism of Ca(2+)-triggered ESCRT assembly and regulation of cell membrane
1128 repair. Nature communications *5*, 5646.
1129 Schneggenburger, R., Meyer, A.C., and Neher, E. (1999). Released fraction and total size of a
1130 pool of immediately available transmitter quanta at a calyx synapse. Neuron *23*, 399-409.
1131 Schneggenburger, R., and Neher, E. (2005). Presynaptic calcium and control of vesicle fusion.
1132 Curr Opin Neurobiol *15*, 266-274.
1133 Schuske, K.R., Richmond, J.E., Matthies, D.S., Davis, W.S., Runz, S., Rube, D.A., van der Bliek,
1134 A.M., and Jorgensen, E.M. (2003). Endophilin is required for synaptic vesicle endocytosis by
1135 localizing synaptojanin. Neuron *40*, 749-762.
1136 Sheehan, P., Zhu, M., Beskow, A., Vollmer, C., and Waites, C.L. (2016). Activity-Dependent
1137 Degradation of Synaptic Vesicle Proteins Requires Rab35 and the ESCRT Pathway. J Neurosci
1138 *36*, 8668-8686.
1139 Shibata, H., Yamada, K., Mizuno, T., Yorikawa, C., Takahashi, H., Satoh, H., Kitaura, Y., and
1140 Maki, M. (2004). The penta-EF-hand protein ALG-2 interacts with a region containing PxY
1141 repeats in Alix/AIP1, which is required for the subcellular punctate distribution of the amino-
1142 terminal truncation form of Alix/AIP1. J Biochem (Tokyo) *135*, 117-128.
1143 Soykan, T., Kaempf, N., Sakaba, T., Vollweiter, D., Goerdeler, F., Puchkov, D., Kononenko,
1144 N.L., and Haucke, V. (2017). Synaptic Vesicle Endocytosis Occurs on Multiple Timescales and
1145 Is Mediated by Formin-Dependent Actin Assembly. Neuron *93*, 854-866 e854.
1146 Suzuki, H., Kawasaki, M., Inuzuka, T., Okumura, M., Kakiuchi, T., Shibata, H., Wakatsuki, S.,
1147 and Maki, M. (2008). Structural basis for Ca2+ -dependent formation of ALG-2/Alix peptide
1148 complex: Ca2+/EF3-driven arginine switch mechanism. Structure *16*, 1562-1573.
1149 Thanawala, M.S., and Regehr, W.G. (2016). Determining synaptic parameters using high-
1150 frequency activation. J Neurosci Methods *264*, 136-152.
1151 Trioulier, Y., Torch, S., Blot, B., Cristina, N., Chatellard-Causse, C., Verna, J.M., and Sadoul, R.
1152 (2004). Alix, a protein regulating endosomal trafficking, is involved in neuronal death. J Biol
1153 Chem *279*, 2046-2052.
1154 Watanabe, S., Mamer, L.E., Raychaudhuri, S., Luvsanjav, D., Eisen, J., Trimbuch, T., Sohl-
1155 Kielczynski, B., Fenske, P., Milosevic, I., Rosenmund, C*., et al.* (2018). Synaptojanin and
1156 Endophilin Mediate Neck Formation during Ultrafast Endocytosis. Neuron *98*, 1184-1197
1157 e1186.
1158

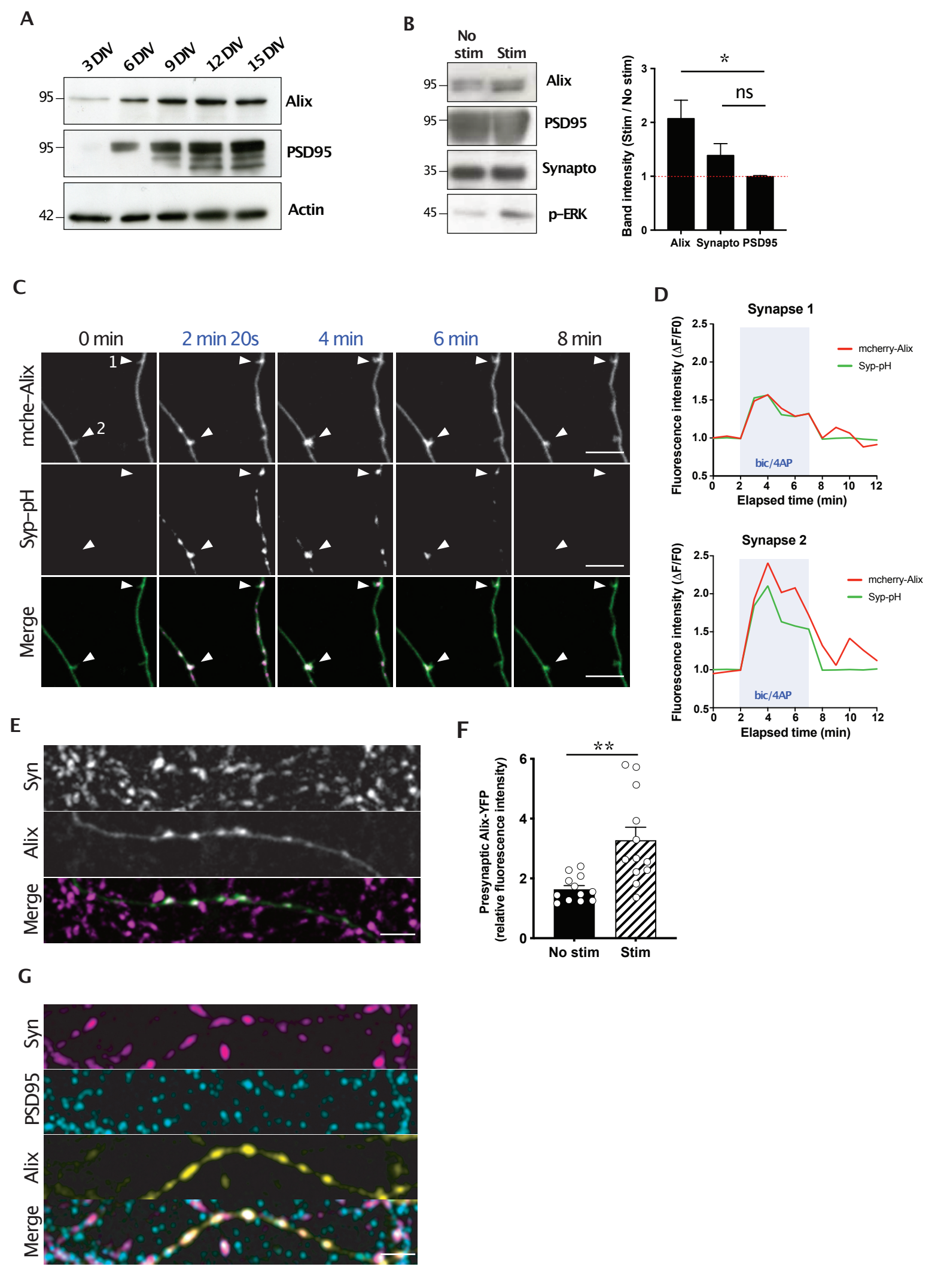
A
3 DIV
6 DIV
9 DIV
12 DIV
15 DIV
95
Alix
95
PSD95
42
Actin
B
No stim
Stim
95
Alix
95
PSD95
35
Synapto
45
p-ERK
Band intensity (Stim / No stim)
*
ns
Alix
Synapto
PSD95
C
0 min
2 min 20s
4 min
6 min
8 min
mche-Alix
Syp-pH
Merge
1
2
D
Synapse 1
Synapse 2
Fluorescence intensity (ΔF/F0)
Elapsed time (min)
mcherry-Alix
Syp-pH
bic/4AP
E
Syn
Alix
Merge
F
Presynaptic Alix-YFP (relative fluorescence intensity)
**
No stim
Stim
G
Syn
PSD95
Alix
Merge

FIGURE1

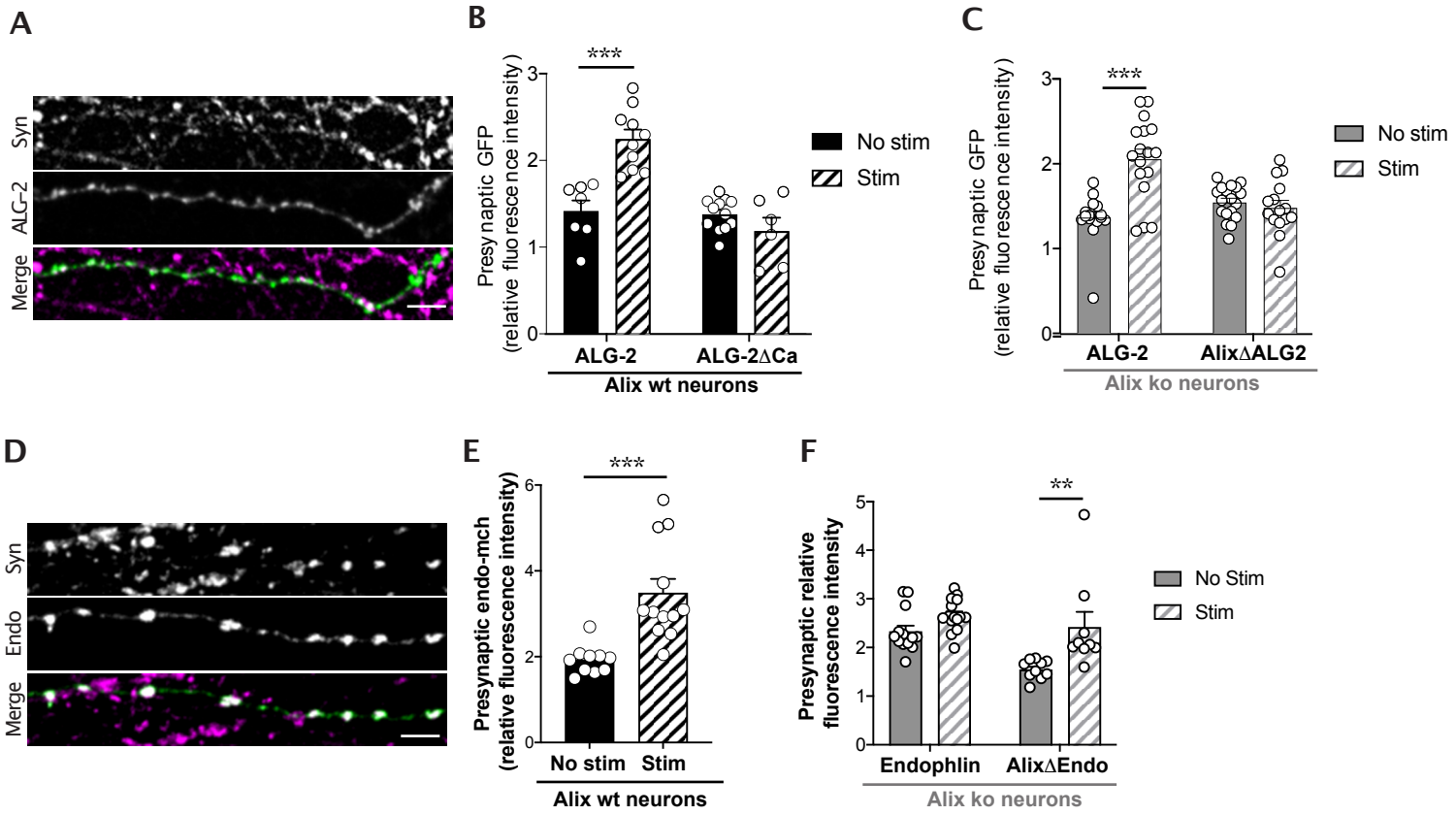
A
Syn
ALG-2
Merge
B
Presynaptic GFP
(relative fluorescence intensity)
***
No stim
Stim
ALG-2
ALG-2ΔCa
Alix wt neurons
C
Presynaptic GFP
(relative fluorescence intensity)
***
No stim
Stim
ALG-2
AlixΔALG2
Alix ko neurons
D
Syn
Endo
Merge
E
Presynaptic endo-mch
(relative fluorescence intensity)
***
No stim
Stim
Alix wt neurons
F
Presynaptic relative
fluorescence intensity
**
No Stim
Stim
Endophlin
AlixΔEndo
Alix ko neurons

FIGURE2

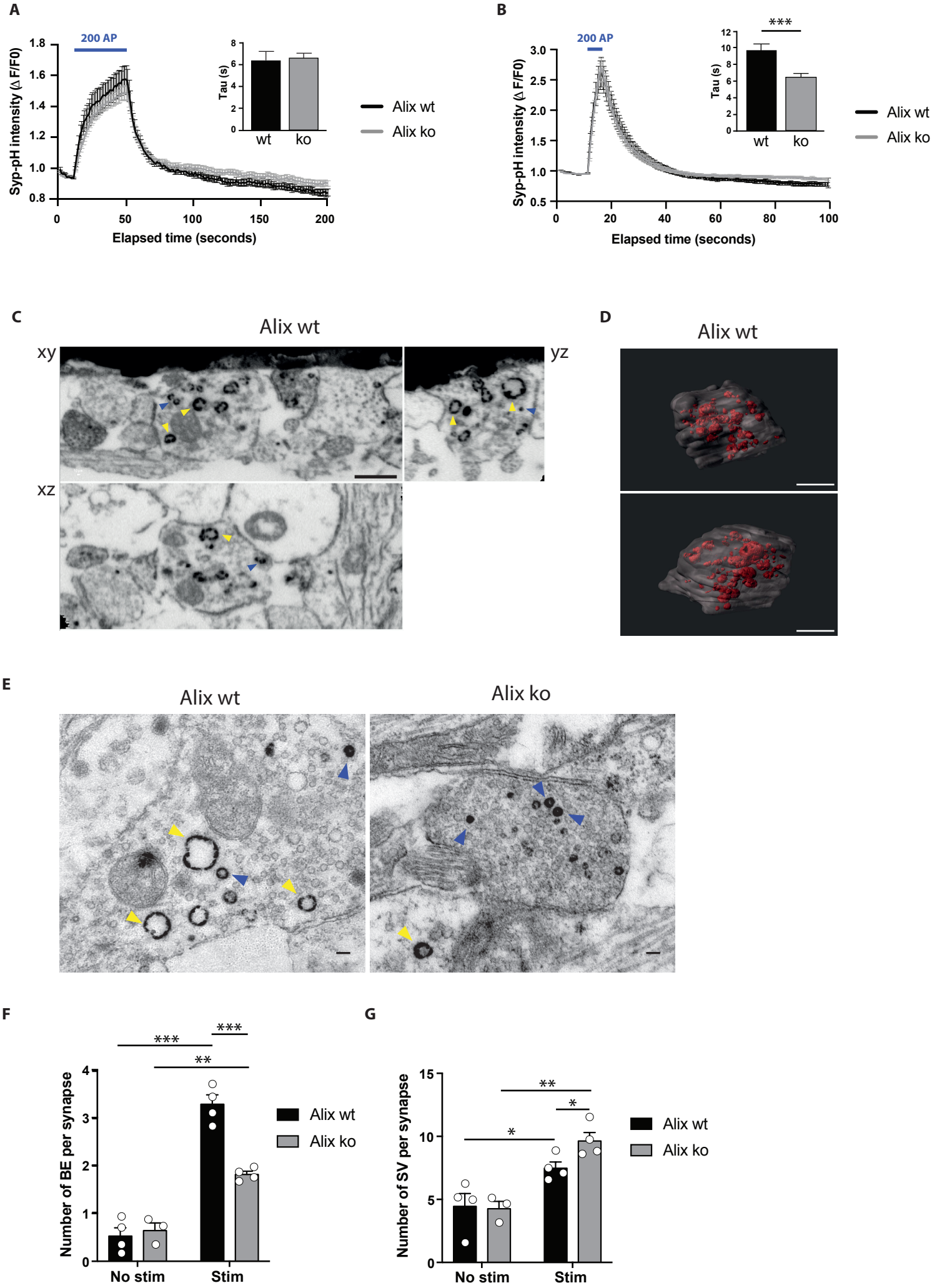
A
200 AP
Syp-pH intensity (Δ F/F0)
Elapsed time (seconds)
Tau (s)
wt
ko
Alix wt
Alix ko
B
200 AP
***
Syp-pH intensity (Δ F/F0)
Elapsed time (seconds)
Tau (s)
wt
ko
Alix wt
Alix ko
C
Alix wt
xy
yz
xz
D
Alix wt
E
Alix wt
Alix ko
F
***
***
**
Number of BE per synapse
No stim
Stim
Alix wt
Alix ko
G
**
*
*
Number of SV per synapse
No stim
Stim
Alix wt
Alix ko

FIGURE3

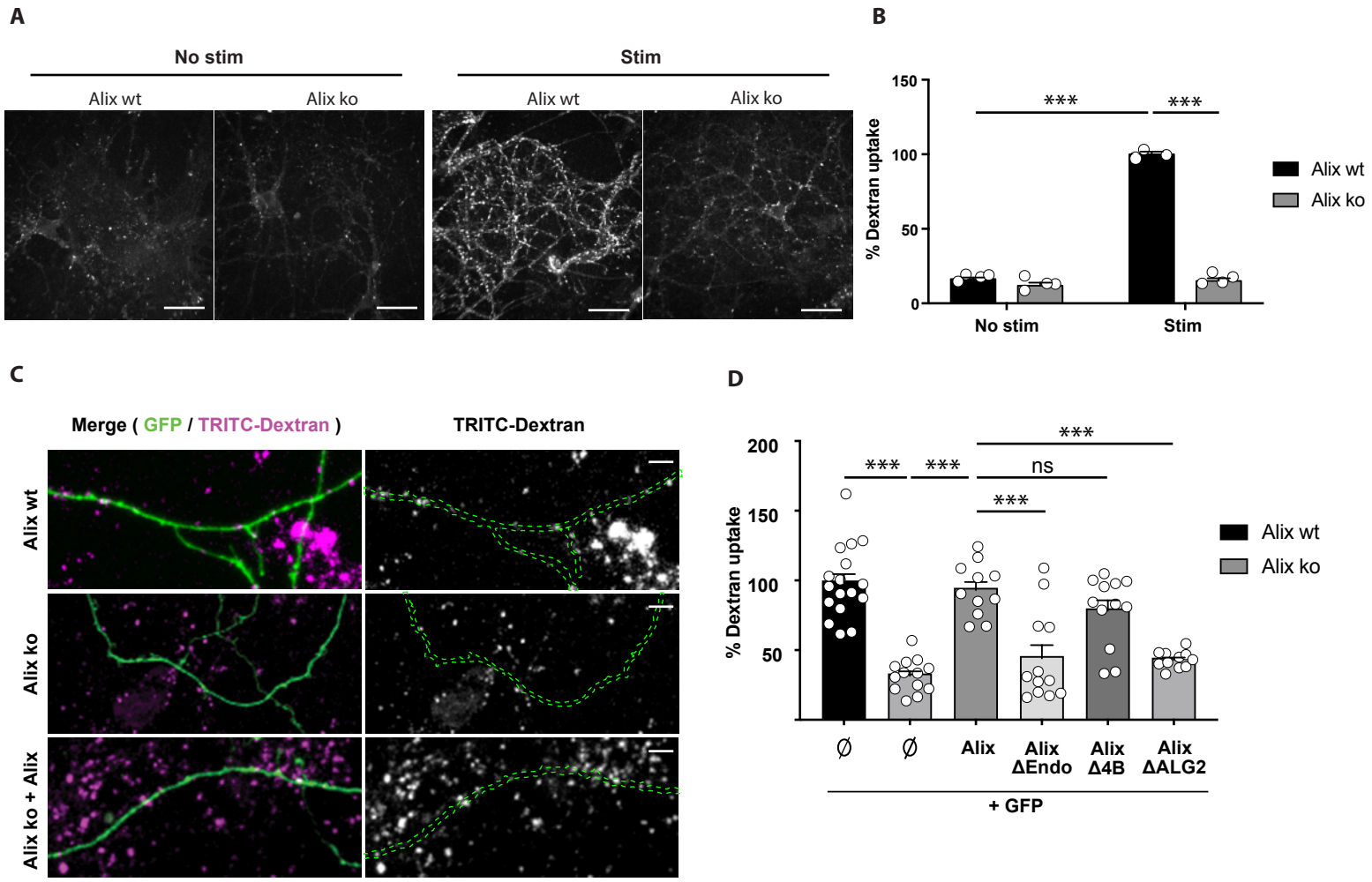
A
No stim
Stim
Alix wt
Alix ko
Alix wt
Alix ko
B
% Dextran uptake
150
100
50
0
***
***
No stim
Stim
Alix wt
Alix ko
C
Merge (GFP / TRITC-Dextran)
TRITC-Dextran
Alix wt
Alix ko
Alix ko + Alix
D
% Dextran uptake
200
150
100
50
***
***
***
ns
Ø
Ø
Alix
Alix ΔEndo
Alix Δ4B
Alix ΔALG2
+ GFP
Alix wt
Alix ko

FIGURE4

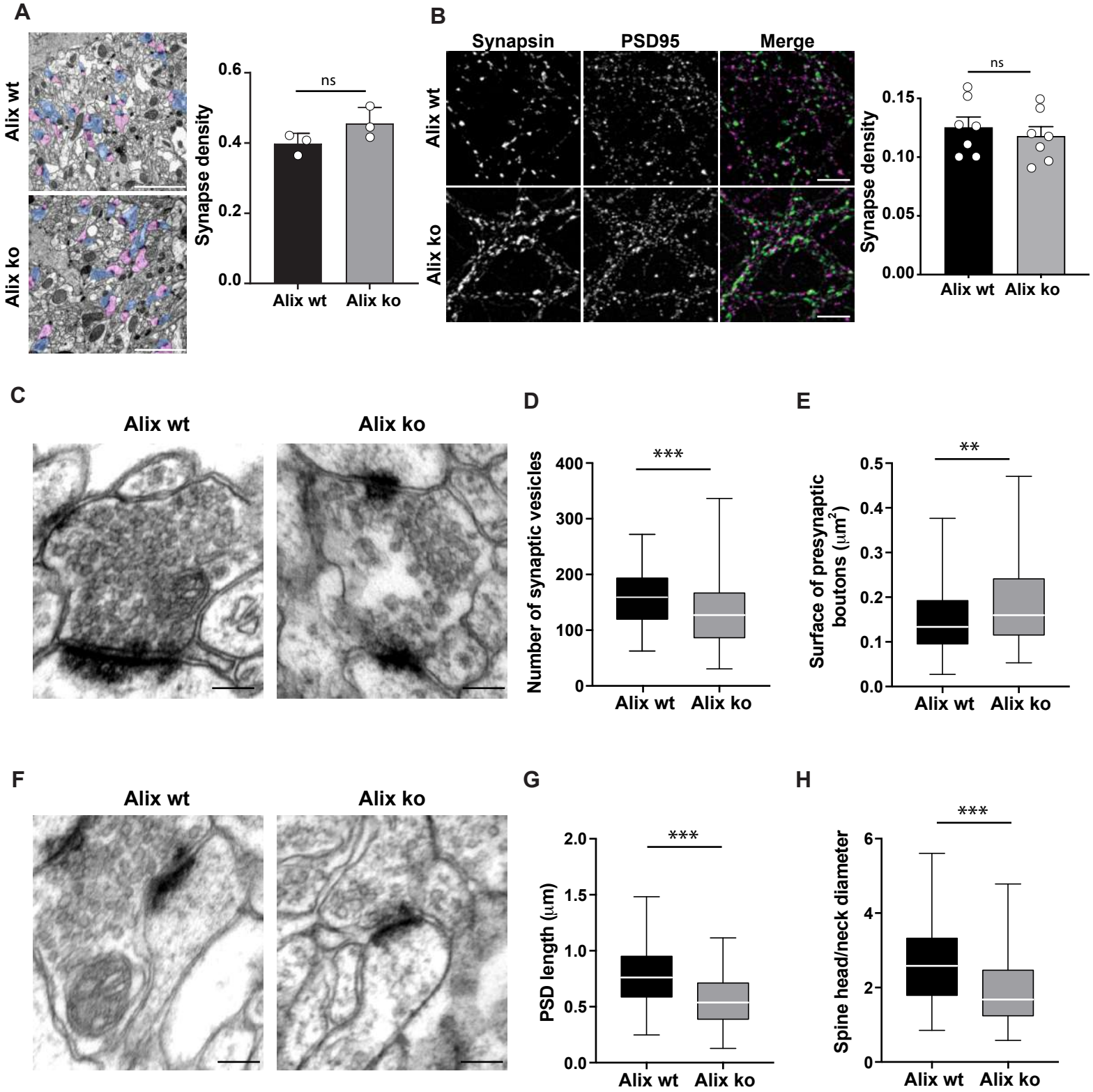
A
Alix wt
Alix ko
Synapse density
0.6
0.4
0.2
0.0
ns
Alix wt
Alix ko
B
Synapsin
PSD95
Merge
Alix wt
Alix ko
Synapse density
0.15
0.10
0.05
0.00
ns
Alix wt
Alix ko
C
Alix wt
Alix ko
D
Number of synaptic vesicles
400
300
200
100
0
***
Alix wt
Alix ko
E
Surface of presynaptic boutons (μm²)
0.5
0.4
0.3
0.2
0.1
0.0
**
Alix wt
Alix ko
F
Alix wt
Alix ko
G
PSD length (μm)
2.0
1.5
1.0
0.5
0.0
***
Alix wt
Alix ko
H
Spine head/neck diameter
6
4
2
0
***
Alix wt
Alix ko

FIGURE5

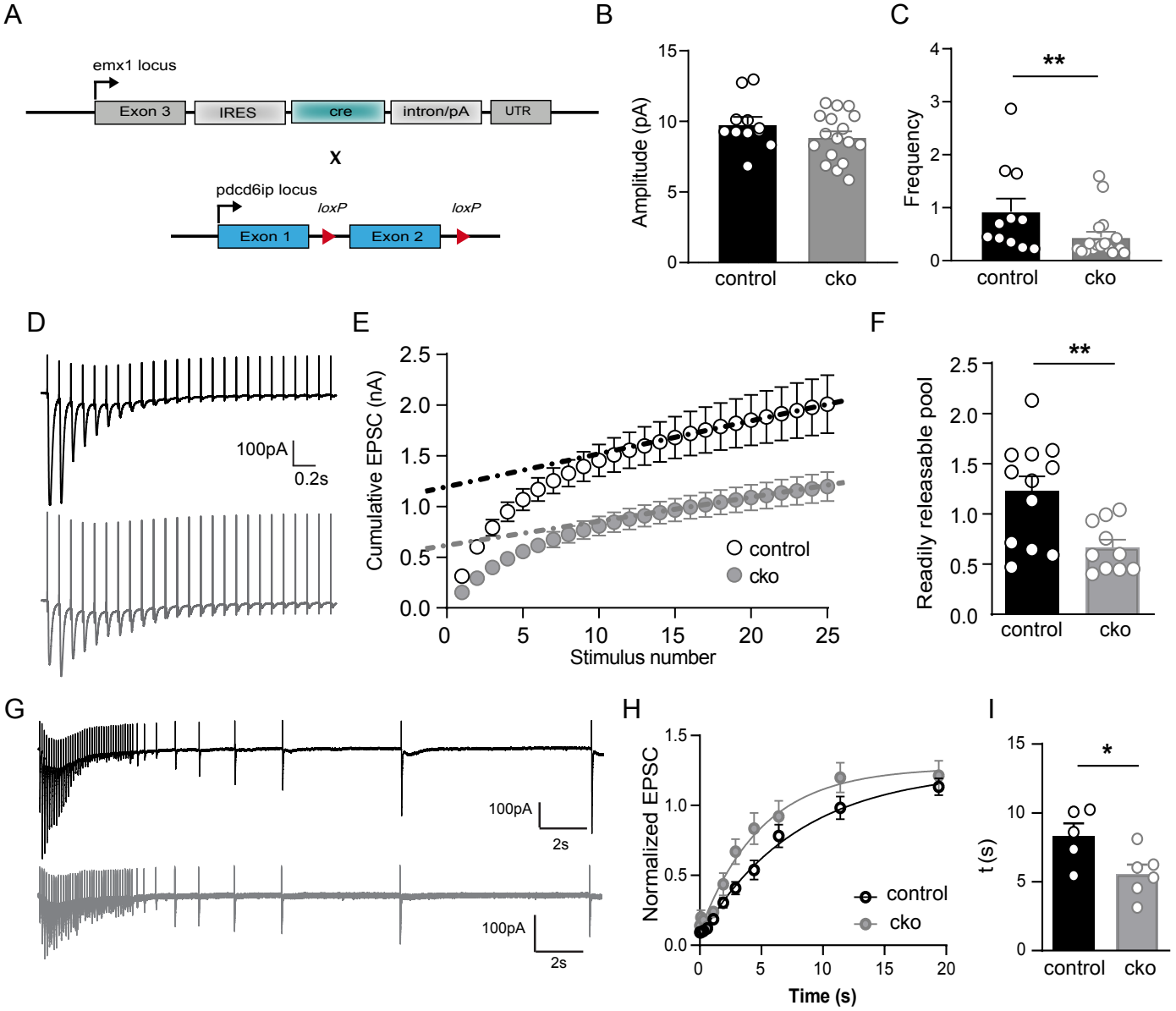
A
emx1 locus
Exon 3
IRES
cre
intron/pA
UTR
x
pdcd6ip locus
loxP
loxP
Exon 1
Exon 2
B
Amplitude (pA)
control
cko
C
Frequency
**
control
cko
D
100pA
0.2s
E
Cumulative EPSC (nA)
Stimulus number
control
cko
F
Readily releasable pool
**
control
cko
G
100pA
2s
100pA
2s
H
Normalized EPSC
Time (s)
control
cko
I
t (s)
*
control
cko

FIGURE6

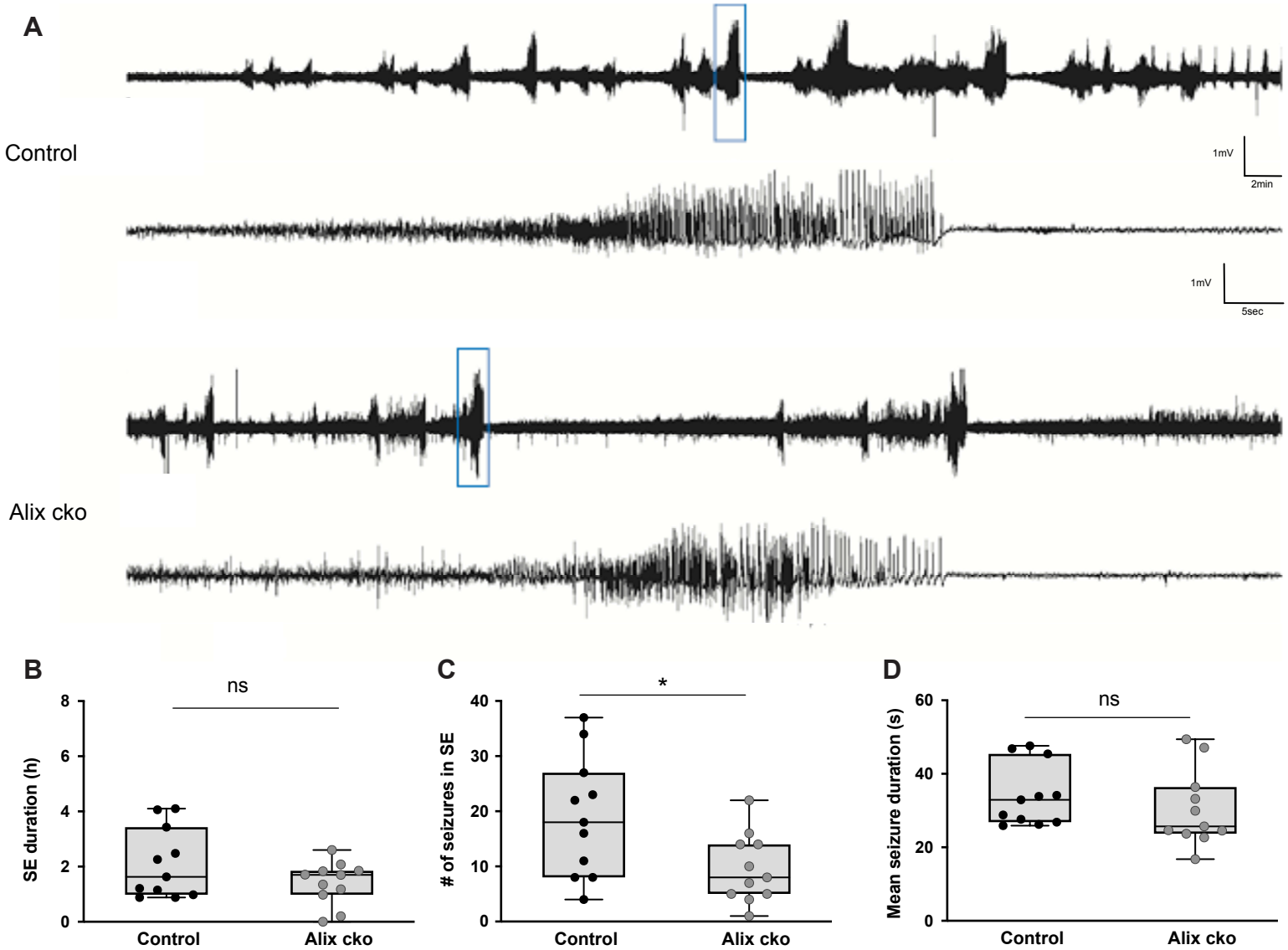
A
Control
1mV
2min
1mV
5sec
Alix cko
B
ns
SE duration (h)
8
6
4
2
0
Control
Alix cko
C
*
# of seizures in SE
40
30
20
10
0
Control
Alix cko
D
ns
Mean seizure duration (s)
60
40
20
0
Control
Alix cko

FIGURE7